Experimental Study of MOS Capacitors as Wireless Radiation Dose Sensors

by

Madusudanan Srinivasan Gopalan

A Thesis Presented in Partial Fulfillment
of the Requirements for the Degree
Master of Science

Approved November 2010 by the
Graduate Supervisory Committee:

Hugh Barnaby, Chair
Keith Holbert
Hongyu Yu

ARIZONA STATE UNIVERSITY

December 2010

ABSTRACT

The RADiation sensitive Field Effect Transistor (RADFET) has been conventionally used to measure radiation dose levels. These dose sensors are calibrated in such a way that a shift in threshold voltage, due to a build-up of oxide-trapped charge, can be used to estimate the radiation dose. In order to estimate the radiation dose level using RADFET, a wired readout circuit is necessary. Using the same principle of oxide-trapped charge build-up, but by monitoring the change in capacitance instead of threshold voltage, a wireless dose sensor can be developed. This RADiation sensitive CAPacitor (RADCAP) mounted on a resonant patch antenna can then become a wireless dose sensor. From the resonant frequency, the capacitance can be extracted which can be mapped back to estimate the radiation dose level. The capacitor acts as both radiation dose sensor and resonator element in the passive antenna loop. Since the MOS capacitor is used in passive state, characterizing various parameters that affect the radiation sensitivity is essential. Oxide processing technique, choice of insulator material, and thickness of the insulator, critically affect the dose response of the sensor. A thicker oxide improves the radiation sensitivity but reduces the dynamic range of dose levels for which the sensor can be used. The oxide processing scheme primarily determines the interface trap charge and oxide-trapped charge development; controlling this parameter is critical to building a better dose sensor.

DEDICATION

To my family

ACKNOWLEDGMENTS

I would like to express my sincere gratitude to my advisor Dr. Hugh Barnaby, for his continuous support and invaluable guidance, during the course of the work. His patience and trust in my capabilities helped me to overcome the pressure of unsuccessful experiments. I am grateful to Dr. Keith Holbert and Dr. Hongyu Yu, my committee members, for their time and efforts to review my work. I would like to thank Barry Wilkens and David Wright for helping me conduct the proton beam experiments and patiently accommodating my experiments on their schedule. I would like to specially thank Craig Birtcher who wire-bonded innumerable samples for my experiments.

I take this opportunity to thank Achal Kathuria, Jonathon Oiler and Ivan Sanchez Esqueda for helping me with the experiments and constructive discussions I had with them

I am indebted to my family for their unconditional love and emotional support throughout my graduate studies. I would also like to thank my room mates Jagdish, Rajesh, Siva and Jaiganesh for their company and emotional support throughout.

TABLE OF CONTENTS

Page

LIST OF TABLES vii

LIST OF FIGURES viii

CHAPTER

1 INTRODUCTION 1

1.1 Historical background 1

1.2 Motivation 1

1.3 Thesis outline and organization 2

2 ELECTRICAL RESPONSE OF MOS CAPACITORS TO RADIATION 4

2.1 Introduction 4

2.2 Parametric shifts due to ionizing radiation 5

3 RADFET DOSIMETERS 8

3.1 Introduction 8

3.2 Principle of operation 8

3.3 RADFET readout circuit 10

3.4 Modes of operation 12

3.4.1 Biased mode 12

3.4.2 Unbiased mode 13

3.5 Parametric dependencies 14

3.5.1 Oxide thickness 14

3.5.2 Oxide processing technique 14

3.6 Limitations of RADFET dosimeter 15

CHAPTER Page

3.7 Low dose resolution 17

3.8 Post-irradiation behavior..... 17

3.9 Major applications..... 18

3.10 Advantages of RADFET dosimeter..... 18

4 MOS CAPACITORS AS RADIATION DOSE SENSORS 20

4.1 Introduction..... 20

4.2 Design of wireless sensor system 20

4.3 Energy band diagram of MOS capacitor..... 21

4.4 Ideal MOS capacitor threshold voltage..... 23

4.5 MOS capacitance – voltage Behavior..... 26

4.6 Non-Ideal capacitance – voltage Behavior..... 29

4.6.1 Fixed oxide charge- Q_f..... 29

4.6.2 Interface trap charge- Q_{it}..... 30

4.7 Extraction of oxide-trapped charge and interface trap charge from C-V curve..... 31

5 THE DOSE PERFORMANCE OF THE RADCAP..... 33

5.1 Processing technique 33

5.1.1 Wet oxidation and dry oxidation 33

5.1.1.1 Experiment results..... 35

5.1.2 Thermally grown high quality oxide..... 41

5.1.2.1 Fabrication steps..... 41

5.1.2.2 Experiment results..... 43

CHAPTER Page

5.2 Dielectric material 46

5.2.1 Experiment results 48

5.3 Impact of oxide thickness 52

5.3.1 Experiment results 52

5.4 Post-irradiation behavior 54

5.5 Discussion on initial precursor hole trap density 56

6 CONCLUSION 58

REFERENCES 59

LIST OF TABLES

Table Page

1. Comparison of sensitivity at zero bias for different oxide processing schemes 15

2. Advantages and disadvantages of conventional dosimeters 19

3. Comparison of properties of silicon nitride and silicon dioxide 47

4. Loss of oxide-trapped charge and midgap voltage shifts resulting from room temperature annealing 56

5. Initial precursor hole trap density estimated from simulation for various processing schemes 56

LIST OF FIGURES

Figure Page

1. Illustration of transport of carriers in oxide 5
2. Impact of oxide-trapped charge and interface trap charge on C-V curves 7
3. Cross section of the RADFET dosimeter 9
4. Illustration of shift in gate voltage in a p-channel RADFET due to radiation 10
5. Measurement setup used to read out the threshold voltage of the RADFET 11
6. Fractional charge yield as function of dose for different ionizing radiation 13
7. Data showing the erasure of oxide-trapped charge due to high temperature annealing 16
8. Energy band diagram of ideal MOS capacitor 22
9. Energy band diagram of MOS capacitor showing potentials and spatial dimension 23
10. Schematic representation of MOS capacitor 26
11. Comparison of ideal MOS C-V curve with experimental data 28
12. Comparison of experimental data with non ideal MOS C-V curve ... 29
13. Illustration of interface states at different biasing conditions in an MOS capacitor 31

Figure Page

14. Pre-irradiation and post-irradiation C-V curves of RADCAP with 100 nm (dry) oxide thickness 36

15. Pre-irradiation and post-irradiation C-V curves of RADCAP with 200 nm (wet) oxide thickness 36

16. Experimental data of normalized oxide-trapped charge density of RADCAP with 100 nm (dry) and 200 nm (wet) oxide thickness 37

17. Experimental data of normalized interface trap density of RADCAP with 100 nm (dry) and 200 nm (wet) oxide thickness 38

18. Comparison of oxide-trapped charge per unit area for RADCAP with 200 nm oxide thickness (wet) obtained from simulation and experimental data 39

19. Comparison of oxide-trapped charge per unit area for RADCAP with 100 nm oxide thickness (dry) obtained from simulation and experimental data 40

20. Comparison of midgap voltage shifts for RADCAP with 200 nm oxide thickness (wet) obtained from simulation and experimental data 40

21. Comparison of midgap voltage shifts for RADCAP with 100 nm oxide thickness (dry) obtained from simulation and experimental data 41

22. Fabrication steps to manufature capacitors using SOI wafers 42

Figure Page

23. Package containing RADCAPs with high quality oxide and the proton beam chamber used for irradiation 43
24. Experimental data showing radiation response of RADCAP with high quality oxide 44
25. Capacitance versus dose map for RADCAP with high quality oxide 45
26. Comparison of oxide-trapped charge per unit area for RADCAP with high quality oxide obtained from simulation and experimental data 46
27. Pre-irradiation and post-irradiation C-V curves of RADCAP with silicon nitride as insulator 48
28. Pre-irradiation and post-irradiation C-V curves of RADCAP with silicon dioxide as insulator 49
29. Comparison of normalized oxide-trapped charge density of silicon nitride and silicon dioxide RADCAP samples as a function of dose 50
30. Ratio of oxide-trapped charge density of silicon dioxide and silicon nitride RADCAP samples as a function of dose 50
31. Comparison of oxide-trapped charge per unit area for silicon nitride RADCAP obtained from simulation and experimental data . 51
32. Comparison of normalized oxide-trapped charge per unit area for RADCAPs with 100 nm, 200 nm oxide thickness as a function of dose 53

Figure Page

33. Comparison of normalized interface state charge per unit area for RADCAPs with 100 nm, 200 nm oxide thickness as a function of dose..... 54

34. Comparison of annealing behavior observed in RADCAPs manufactured using different processing techniques..... 55

Chapter 1

INTRODUCTION

1.1 Historical background

The RADiation sensitive Field Effect Transistor (RADFET) has been used as a radiation dose sensor for the past 30 years [1-3]. They find their use in various applications like unmanned satellites, nuclear industry and radiotherapy. These sensors measure total ionizing dose through radiation induced threshold voltage shifts. These shifts are due to build-up of fixed charge in the sensitive gate oxide during radiation exposure [2-5]. The dose sensitivity and dynamic range of these sensors have been well studied [3-9]. As compared to other conventional techniques, these sensors are fairly low power [5], and are easily integrated into electronic instrumentation. Nevertheless RADFETs require some power to operate and, in most applications, are wired directly to readout circuitry which must be resistant to radiation damage. Efforts to develop wireless radiation dose sensors have gained momentum especially in the field of radiotherapy. RADPOS, a wireless dose sensor, uses an RF position system to record dose and position within the patient simultaneously [7]. The cost of these systems limits their usage in other general purpose radiation detection applications. Defense and nuclear security applications also benefit from the use of wireless radiation sensors, where remote, convert detection at standoff range are much desired features.

1.2 Motivation

The threat of an attack with radiological or nuclear materials has increased so much that monitoring the movement of radioactive material is imperative.

Unfortunately critical gaps exist in the ability to detect and disrupt pathways for these types of Weapons of Mass Destruction (WMDs). While active detection methodologies provide some advantage in this arena, neutron or gamma radiography comes at the cost of introducing additional man-made radiation. Moreover, the complexities of active systems make them difficult to be used unattended or without being revealed. Ideally these systems should be somewhat low in cost, small in size, require little to no power and operate wirelessly. This would allow an array of such sensors to be embedded into surface coatings and used to monitor a multitude of pathways for hazardous nuclear material in and out of the country. Such attributes would also be advantageous for medical applications, particularly sensors monitoring radiation dose during cancer radiotherapy. For example, a detector mesh conforming to a tumor volume could be constructed of miniaturized passive detectors to provide real time verification of the radiation dose delivered. This type of in-vivo dose verification could significantly reduce the possibility of overdose to healthy tissue and minimize the possibility of severe misadministration of high dose rate radiation.

A sensor with these specifications may be realized with a solid state RADiation sensitive CAPacitor (RADCAP) mounted on a resonant patch antenna. In order to develop the RADCAP it is necessary to understand and control the different parameters influencing its radiation sensitivity.

1.3 Thesis outline and organization

The organization of the thesis is as follows: Chapter 2 presents the general impact of radiation on the operation of solid state MOS capacitors. Chapter 3

reviews the operating principle of the RADFET dosimeter. Chapter 4 presents the technique to use RADCAP as a radiation dose sensor that can be used for remote wireless sensing applications. The influence of different parameters on the operation and sensitivity of MOS capacitors to ionizing radiation is discussed in Chapter 5. Chapter 6 summarizes the key contribution of this thesis.

Chapter 2

ELECTRICAL RESPONSE OF MOS CAPACITORS TO RADIATION

2.1 Introduction

The major impact of radiation on MOS devices is the build-up of fixed charge in the insulator beneath the gate of the device. Due to build-up of fixed charge, the electrical characteristics of the device changes. Most modern MOS structures have silicon dioxide (SiO_2) as the insulator. When a MOS device is exposed to ionizing radiation, energy is deposited in the oxide. The amount of energy deposited depends on the Linear Energy Transfer (LET) of the primary or secondary particles that pass through the oxide material. This energy creates electron-hole pairs which move under the influence of the applied electric field. Since the mobility of electrons in oxides is much higher than holes, electrons are swept out by the applied or intrinsic electric field while holes move slowly in the direction of the field. Some of the holes become trapped in the oxide and form fixed positive charge. This charge causes the flat-band voltage of the MOS system to change, which, for the MOS capacitor, is manifested as a negative shift in the capacitance vs. voltage (C-V) curve. The damage caused by irradiation is dependent on temperature, oxide thickness, applied field and oxide processing techniques.

One of the most important factors affecting the dose response of a MOS system is the Si/SiO_2 interfacial properties. As oxides are grown, oxygen diffuses to the interface where it reacts with the bulk silicon. Not all of silicon atoms at the interface are oxidized which leaves some dangling bonds at the interface. These

dangling bonds at the interface give rise to interface states in the band gap which affect the shape of the C-V curve. In addition to dangling bonds, oxygen vacancies in the bulk of the dielectric, typically result during processing. The vacancies are considered to be the primary precursor defects which trap holes during radiation exposure. It is important to study the impact of different oxidation techniques on the formation of interface traps and oxygen vacancies since they determine the radiation sensitivity of the MOS capacitor.

2.2 Parametric shifts due to ionizing radiation

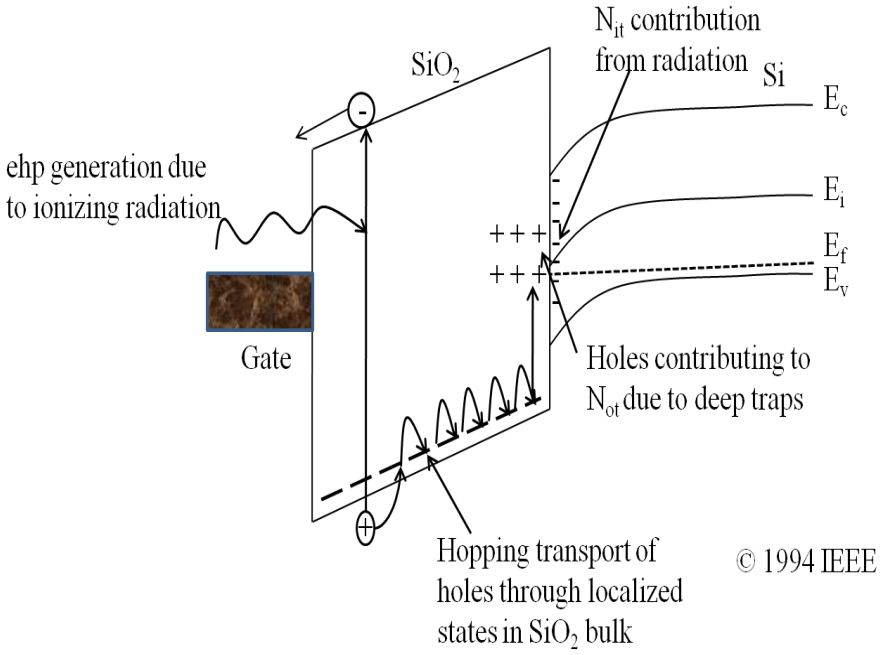

Fig. 1. Illustration of transport of carriers in oxide

The processes involved in the generation, transport and trapping of holes are illustrated in Fig. 1 [11]. Holes, after being generated in the oxide transport through hopping processes in the presence of the electric field. Depending on the direction of the field, holes move either towards or away from Si/SiO_2 interface.

When the electric field across the oxide points towards the Si/SiO_2 interface the impact of ionizing radiation is maximized. After the holes reach the interface, they get trapped in oxygen vacancies and cause voltage shifts in the C-V curve. Most vacancies are close to but not at the interface [11] and are very sensitive to oxide processing conditions. In some cases, holes can react with other species in the oxide. These species, typically protons, can transport to the interface and create interface traps, which cause deleterious effects in MOS C-V curves.

The presence of oxide-trapped charge and interface traps alters the C-V characteristics of a MOS capacitor. The threshold voltage of a MOS capacitor is given as

$$V_{th} = V_{th}^{0} + \Delta V_{th}(t), \tag{2.1}$$

where V_{th}^{0} is the threshold before irradiation and $\Delta V_{th}(t)$ is the shift caused by radiation. This change in threshold voltage, has the following contributions

$$\Delta V_{th}(t) = \Delta V_{OT}(t) + \Delta V_{IT}(t), \tag{2.2}$$

where $\Delta V_{OT}(t)$ is the shift in threshold voltage due to trapped holes (i.e., oxide-trapped charge), while the change, $\Delta V_{IT}(t)$, is due to charged interface traps. Trapped holes and interface traps both contribute to, not only threshold voltage alterations, but the total voltage shift observed in the C-V curves. The voltage shift due to oxide-trapped charge and interface trap charge can be expressed as

$$\Delta V_{OT} = -\frac{q}{C_{ox}} \Delta N_{OT}(t), \tag{2.3}$$

$$\Delta V_{IT} = \frac{(-\Delta Q_{IT})(t)}{C_{ox}}, \tag{2.4}$$

where q is the electronic charge and C_{ox} is the oxide capacitance per unit area. Positive oxide-trapped charge (N_{OT}) always causes negative (left) shifts in the C-V curve. Interface traps contribute to net negative or positive charge at the Si/SiO_2 interface depending on the position of the Fermi level relative to the intrinsic energy level at the interface. Consequently, the threshold voltage offset is directly proportional to the number of holes trapped in the deep traps near the interface and the net contribution from charged interface states, Q_{IT}.

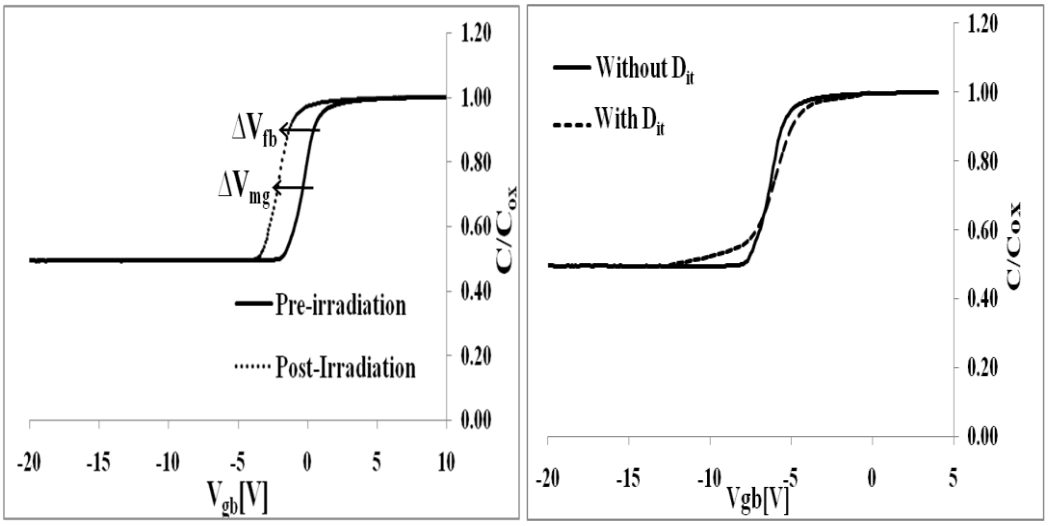

Fig. 2. Impact of oxide-trapped charge and interface trap charge on C-V curves

Fig. 2 shows the simulation results for pre-irradiation and post-irradiation shift only due oxide-trapped charge which is ΔV_{OT} in Equation 2.3. The shift reported in the figure is at a radiation dose level of 100 krad. Fig. 2 also shows the effects of charged interface states Q_{IT} in the silicon band gap contributing to the change in shape of the curve. The above parameters and their dependence are very important as they characterize the post-irradiation behavior of the device.

Chapter 3

RADFET DOSIMETERS

3.1 Introduction

A conventional way to measure the amount of dose is by using a RADiation sensitive Field Effect Transistor (RADFET) [1]. The RADFET dosimeter was developed in 1970 and has been widely used in the aerospace, medicinal and nuclear industries. The dosimeter is a MOS field effect transistor specially designed to trap holes in the insulator beneath the gate, but not exhibit measurable interface trap buildup. The electrical shift in the threshold voltage of the RADFET is calibrated to measure ionizing radiation dose. The RADFET is typically engineered such that its threshold voltage shifts linearly over the wide range of dose levels. The RADFET dosimeter became popular since it is compact and can be readily included with other electronic instrumentation. They typically find their usage as wired radiation dose sensors with readout circuits attached to them.

3.2 Principle of operation

Fig. 3 is an illustration of RADFET cross-section. Like all MOSFETs, it is composed of a MOS capacitor separating drain and source terminals. The controlling gate terminal is deposited above an insulator, which is usually an amorphous oxide film (or oxide-nitride composite) with a thickness of around 0.1-0.2 μm [2]. Similar to the radiation process described in the previous chapter for the MOS capacitor, holes generated in the oxide get trapped in the oxide and cause a shift in the threshold voltage (ΔV_T) of the device. The buildup of net

positive oxide-trapped charge (N_{OT}) is a function of the total dose, D, the oxide film thickness, t_{ox} and gate bias during irradiation. To first order, N_{OT} buildup can be assumed to be proportional to D and t_{ox}. The functional relationship of N_{OT} to gate bias is more complex but it is monotonically increasing.

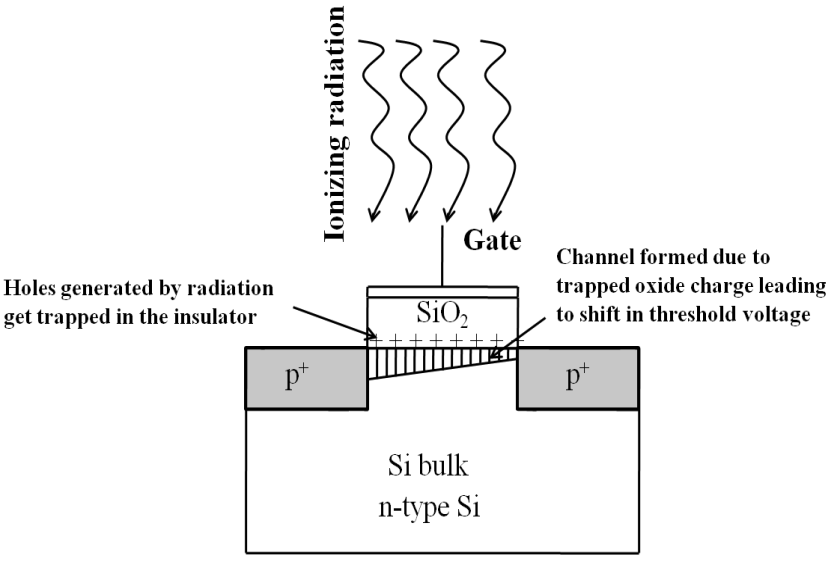

Fig. 3. Cross section of the RADFET dosimeter

The relationship between threshold voltage and the above parameters is given by [3]

$$-\Delta V_T = \frac{t_{ox} q N_{OT}}{\varepsilon_{ox}\varepsilon_0} + f(N_i) + g(t), \qquad (3.1)$$

where N_{OT} is the density of positive trapped charge during irradiation, q is the electronic charge, ε_{ox} is the dielectric constant of oxide, ε_0 is the permittivity of free space, $f(N_i)$ is the term to account for the effects of interface traps, and g(t) is trapped charge annealing term. The shift in threshold voltage is linear until it begins to saturate at a particular dose. The saturation dose is a function of the density of trapping sites (oxygen vacancies) in oxide and gate bias under

irradiation. Fig. 4 shows the shift in the drain current vs. gate voltage (I_D-V_G) characteristics of a p-channel RADFET [3]. As previously mentioned this shift is monitored to sense the radiation dose exposure at the RADFET's spatial location.

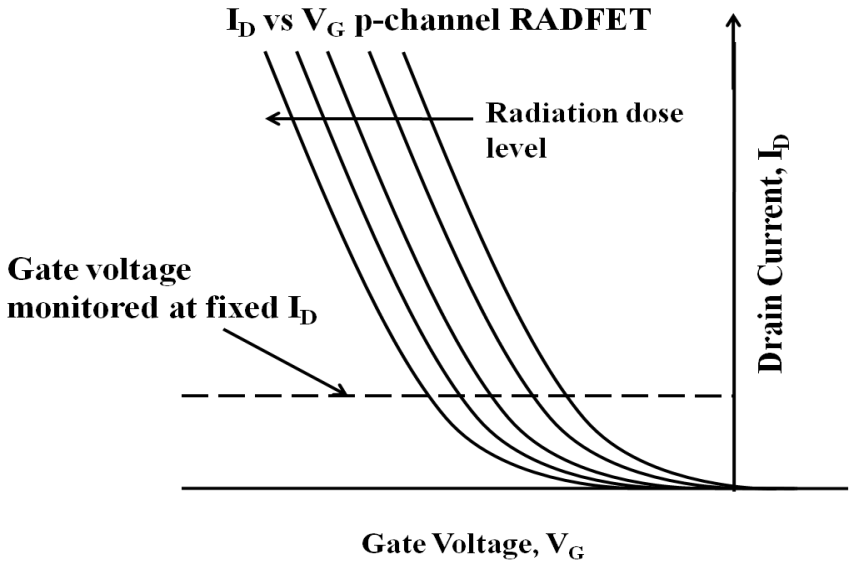

Fig. 4. Illustration of shift in gate voltage in a p-channel RADFET due to radiation

3.3 RADFET readout circuit

The unit to measure the dose of ionizing radiation is the rad, which denotes the energy absorbed per unit mass in the target material. The RADFET dosimeter can be used to sense dose levels in the order of tens of rads to kilorad levels [3]. The dosimeter can be designed to give a linear shift in threshold voltage, V_T as a function of dose for the required range of dose levels. The change in the threshold voltage is typically obtained by monitoring the source voltage at fixed drain current I_D through the device. A simple readout configuration is shown in Fig. 5. The circuit contains a constant current source I_{SS} and measures the change in gate-to-source voltage, which is a function of the threshold voltage.

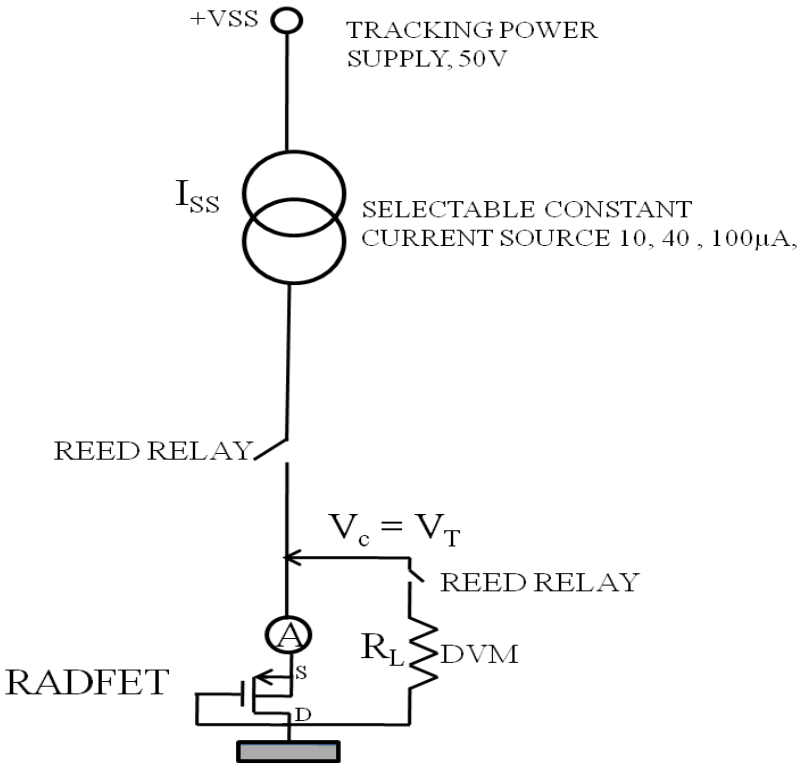

Fig. 5. Measurement setup used to read out the threshold voltage of the RADFET

The technique to measure the shift in threshold voltage is to calculate the source to gate voltage (V_{SG}) that is required to obtain I_D through the device [4]. The drain current I_D through the device is given by the following equation

$$I_{D,pre-rad} = K_p' \frac{W}{L}(V_{SG1} - |V_{t1}|)^2, \tag{3.2}$$

$$I_{D,post-rad} = K_p' \frac{W}{L}(V_{SG2} - |V_{t2}|)^2, \tag{3.3}$$

where $K_p' = \frac{1}{2}\mu_p C_{ox}$, μ_p is the mobility of holes, C_{ox} is the oxide capacitance per unit area, $I_{D,pre-rad}$ is the drain current prior to irradiation, $I_{D,post-rad}$ is the drain current after irradiation, V_{SG1} is the source to gate voltage prior to irradiation, V_{t1} is the threshold voltage prior to irradiation, V_{SG2} is the source to gate voltage post-

irradiation, V_{t2} is the threshold voltage post-irradiation, W, L are channel width and length of the RADFET respectively. The drain current through the device is kept constant using the current source I_{SS}. By equating the right hand side of Equations 3.2 and 3.3, the following equation is obtained

$$K_p^{'} \frac{W}{L}(V_{SG1} - |V_{t1}|)^2 = K_p^{'} \frac{W}{L}(V_{SG2} - |V_{t2}|)^2 . \quad (3.4)$$

Cancelling the common terms and taking square root on both sides,

$$V_{SG2} - V_{SG1} = |V_{t2}| - |V_{t1}| . \quad (3.5)$$

The change in V_{SG} at different dose levels that produces I_D is a direct representation of shift in threshold voltage ΔV_T thereby enabling easy read out of the dose level.

3.4 Modes of operation

3.4.1 Biased mode

In order to improve the hole trapping efficiency in oxide, a fixed electric field is applied during irradiation. This field improves the charge yield for the same dose levels thereby resulting in an increase in oxide-trapped charge buildup ΔN_{OT}. The applied electric field also extends the linearity of the threshold voltage shift [5] as a function of dose. As the internal field caused by the space charge opposes the applied field, carriers do not separate as readily and this can result in saturation of ΔN_{OT} with dose. The general principle to design a RADFET dose sensor working in the presence of electric field is to reduce the thickness of oxide thereby increasing the electric field [5]. The thinner oxide yields higher electric fields but inherently is less radiation sensitive compared to thicker oxides. The

tradeoff is to use a slightly thinner oxide with bias thereby improving the dynamic range of the dosimeter sacrificing its sensitivity.

3.4.2 Unbiased mode

The unbiased mode is used in applications where the sensitivity can be sacrificed for improved dynamic range of the sensor. This enables the sensor to measure high doses and work in the absence of electric field, power supply etc. In order to read out the dose value, wired processing circuitry is typically utilized. The general principle to design sensors working in unbiased mode is to increase their oxide thickness [6, 7] thereby improving its sensitivity.

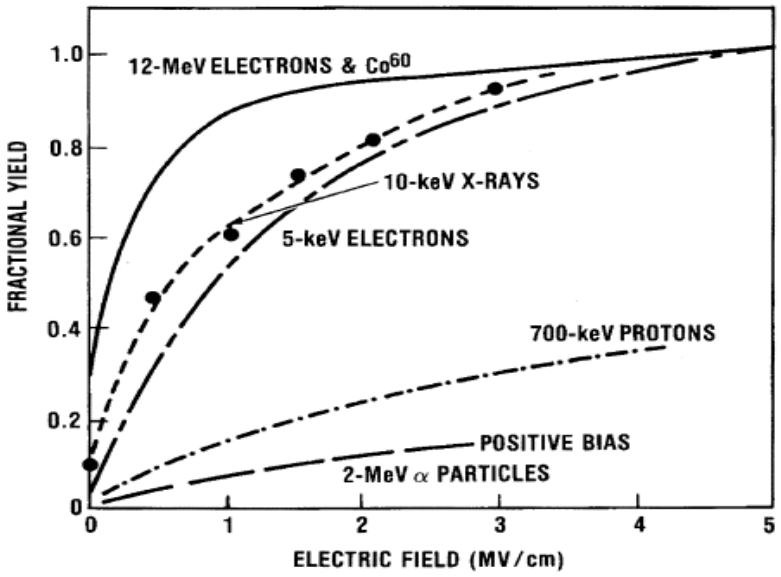

Fig. 6. Fractional charge yield as function of dose for different ionizing radiation

Shown in Fig. 6 is the charge yield curve for different ionizing radiation sources as a function of electric field [11]. The yield at zero bias is lower and this impacts the sensitivity of the dosimeter.

3.5 Parametric dependencies

3.5.1 Oxide thickness

The sensitivity of the dose sensor is directly proportional to the thickness of the oxide. In order to make dosimeters that are more sensitive to radiation, the thickness of oxide t_{ox}, is a critical parameter. The trapped hole density N_{OT} is controlled by the density of precursor traps, N_D, in the oxide. As noted above these precursors are typically oxygen vacancies. From [2] it is known that the thickness t_{ox} is proportional to N_{OT}, implying that an increase in oxide thickness results in a better radiation sensitive device. The oxide thickness cannot be increased indefinitely, because this would reduce the electric field and hence the charge yield.

3.5.2 Oxide processing technique

The oxide film in the RADFET controls the sensitivity and stability of the dosimeter. Higher sensitivity is quantified by large changes in trapped charge for a given radiation dose. This requires the control of charged species in the oxide [8] namely ionic impurity, hole and electron traps and interface states at the silicon/insulator interface. The different processing schemes that are used to grow oxides are wet oxidation, dry oxidation and chemical vapor deposition. Dry oxidation is used for thinner oxides while wet oxidation is used for thicker oxides. Table 1 from [8] compares the sensitivity of oxide at zero bias based on their thickness and processing scheme.

T_{ox}, µm	Oxide type	Sensitivity at zero bias, mV/rad
0.12	Dry O_2	0.06
0.2	Dry O_2	0.18
0.25	Wet O_2	0.16
0.5	Wet O_2	0.5
0.85	Wet O_2	1.2
0.9	Wet O_2	1.28
0.94	Wet O_2	1.64
1.12	Dry + CVD	2.4
1.26	Wet O_2	2.2

Table 1. Comparison of sensitivity at zero bias for different oxide processing schemes

It can be seen from the table that thicker oxides are more sensitive than thinner oxides. Chemical vapor deposition (CVD) yields highly radiation sensitive oxides but results in poor uniformity in thickness [8]. A very good control of the process is essential to make a radiation sensor that meets the required specifications.

3.6 Limitations of RADFET dosimeter

A dose sensor is characterized by its measurement accuracy and minimum measurable dose level that indicates the sensor's sensitivity. Read time instabilities, temperature and noise limit the usage of RADFET as a reliable dose sensor under certain conditions. Read time instabilities are due to the creation of interface states at the silicon/insulator interface. The threshold voltage shift ΔV_T is known to drift up [3-5] immediately after the read bias is applied. This contributes to about 1% error in the total ΔV_T measured. This error can be reduced by reading the measurements from the device a few minutes after applying the read bias. The threshold voltage of the RADFET decreases with increasing temperature. The threshold voltage shifts seen before and after irradiation also have an error due to variation in temperature and this impacts the measurement

accuracy. The error caused by temperature fluctuations can be reduced by biasing the device at I_D^0 which is the zero temperature coefficient point [9]. The sensitivity of the sensor is severely impacted if the operating temperature of the ambient is above 150°C. The trapped positive charge in the insulator is annihilated by heating the sample to 250-300°C for 45 minutes and results in erasure of the stored charge. Fig. 7 shows the results of high temperature annealing on irradiated devices and it can be seen that the oxide-trapped charge is erased as shown by a shift in C-V characteristic. The final factor limiting the minimum measurable dose is the signal to noise ratio. The 1/f noise limits the performance of the dose sensor at low dose levels. From [5] it is known that an increase in area reduces the noise contribution and yields an improvement factor of greater than 50.

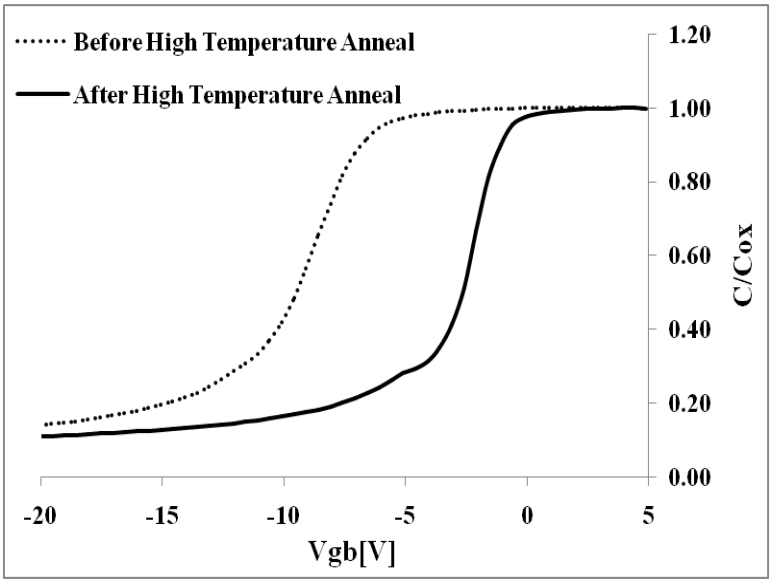

Fig. 7. Data showing the erasure of oxide-trapped charge due to high temperature annealing

3.7 Low dose resolution

The readout circuit can process threshold voltage changes of around 1 mV very accurately. However, due to the drift of the threshold voltage when the read bias is applied [3-5], a 1 mV shift in threshold voltage cannot be used as a signal. The initial drift depends on the properties of the silicon/insulator interface and is present at all temperatures. The readout circuitry can have the correction circuit since this drift is well modeled and predictable. In order to estimate the resolution for low doses, the drift is measured and corrected. A fraction of this drift multiplied by 10 is the minimum acceptable threshold voltage shift that is processed. RADFET dosimeters typically can measure dose levels of the order of one rad very easily and by using thicker oxide, this value can be decreased further.

3.8 Post-irradiation behavior

Even after the irradiation stops the threshold voltage continues to drift with time. The magnitude of the drift depends on temperature, applied bias during and after irradiation and total dose of exposure. The drift of the threshold voltage is due to tunneling of electrons from the substrate which annihilate trapped holes and slow states at the silicon/insulator interface. The electron tunneling is highly dependent on the oxide processing scheme and is known to decrease with thicker oxides [5]. The fading phenomenon is reproducible and can be taken into account enabling proper calibration. This fading effect is enhanced by low dose rate [10] and degrades the accuracy of the dosimeter.

3.9 Major applications

The RADFET dosimeter finds its major application in aerospace industry. The first dosimeter used in a space application was in 1978 [5] and it has been used ever since. The information from the dosimeter can be used to assess the radiation-induced changes in device circuit's performance thereby predicting its failure point. The RADFET dosimeter also finds its application in the nuclear industry. Since the dose levels to be measured range from 1 krad to 1 Mrad [5] they are used in biased mode to provide real-time dose readings. One of the other major applications of the RADFET is in radiotherapy to measure the amount of dose delivered. In-vivo dosimetry is used in radiotherapy departments to check the amount of dose delivered to the patient. The major impetus that has been driving the use of RADFET dosimeter is its better accuracy and lower cost.

3.10 Advantages of RADFET dosimeter

The electrical nature of the output signal combined with its relatively small size and ease of manufacturing motivate the use of RADFET dosimeters. The measurement of dose information from the sensor is non-destructive and the oxide surface holds the charge for several years without fading off. There is no external circuit needed to store the dose information. Since the sensing signal is a change in the threshold voltage, the power dissipation of the sensor is very small and makes it attractive compared to its counterparts which need high voltage power supplies [3]. Table 2 summarizes the advantages and disadvantages of conventional dosimeters [3].

CLASS OF DOSIMETER	DATA PROVIDED	ADVANTAGES	DISADVANTAGES
Ionization Tubes	rad (air)	Standard Medium Good Signal	Needs HV power supply, Large
Scintillators	flux	Precise	Needs HV power supply, Large
Silicon diodes	flux	Small, remote reading	Very small signals
TLDs	rad (LiF)	Small	Destructive read, not remote reading
Glass	rad (Si,O,X)	Small dc signal	Optics required
Plastic	rad (C,H)	Small dc signal	Optics required
MOS	rad(SiO_2)	Ultra small dc signal	Accuracy at low doses, requires electrical bias
Other space charge methods	rad	Dc signal, wide choice of medium	Development required

Table 2. Advantages and disadvantages of conventional dosimeters

Chapter 4

MOS CAPACITORS AS RADIATION DOSE SENSORS

4.1 Introduction

In the past decade, which has seen many technological advancements and breakthroughs, the risk of nuclear attack has significantly gone up. With the establishment of the Domestic Nuclear Detection Office (DNDO) in 2005, the U.S. Department of Homeland Security is tasked with development of a "robust" and "layered" system to guard against attacks on the Nation involving the use of nuclear or radiological devices. The DNDO specifies that the "layered" defense should include capabilities to detect illicit movement of nuclear and radiological material overseas and to enhance domestic detection and interdiction efforts. One approach to detect radiation despite shielding is to physically locate detection devices in the vehicle during transit, thereby increasing the time-integrated signal. Passive detection systems may address these concerns by enabling the installation of large distributed sensor networks that are unattended and "hidden."

4.2 Design of wireless sensor system

One passive sensor that may be suitable for these types of detection systems is a micro-chip composed of a resonant patch antenna which is loaded by a RADiation-sensitive CAPacitor (RADCAP). The capacitor operates as an ionizing radiation detector in ways similar to the RADFET. The capacitively-loaded patch resonator chip can be illuminated by sweeping an RF source over a bandwidth of frequencies. The capacitor is designed such that the nominal value resonates the patch antenna at the center frequency of the RF sweep. The value of

the capacitance at the antenna terminals is therefore a function of ionizing radiation dose. As the source sweeps over the band, the antenna array receives the energy and scatters it back out towards the source. The electromagnetic signature of the device is recorded by a specially designed receiver, the RF interrogator. The peak of reflected response is at the frequency of resonance. Since the properties of the antenna are known, the capacitance at the antenna terminals is easily calculated from the resonant frequency. This capacitance, in turn, is used to find the ionizing radiation dose. The novelty of the design is in using a single capacitor to act as both an ionizing radiation detector and resonator element in a passive patch antenna loop. In order to build a capacitor that is sensitive to radiation, one has to understand the operation of a MOS capacitor and the various parameters that could be important to improve its sensitivity.

4.3 Energy band diagram of MOS capacitor

The energy band diagram of an ideal MOS capacitor is shown in Fig. 8. Aluminum forms the metal gate with silicon dioxide forming the insulator and the p-type Si is the semiconductor. The aluminum work function $q\phi_{Al}$ is the difference between free electron energy level E_0 and the Fermi level $E_{f_{Al}}$. The silicon work function is

$$q\phi_{Si} = q\chi_{Si} + (E_c - E_f), \tag{4.1}$$

where $q\phi_{Si}$ is the silicon work function, $q\chi_{Si}$ is the electron affinity of silicon, E_c and E_f are the conduction band and valence band energy levels respectively. The metal has a higher work function than semiconductor and the electrons will

transfer instantaneously from the metal side to the semiconductor to establish thermal equilibrium. Thus the aluminum layer will have a thin layer of holes while the semiconductor side will have acceptor ions (N_a^-) to compensate them. This causes the bands to bend and since $\xi = \frac{1}{q}\frac{dE_c}{dx}$, this results in a positive electric field ξ across the oxide.

In order to compensate the difference in the work functions of the metal and the semiconductor, a voltage needs to be applied. This voltage is called flat-

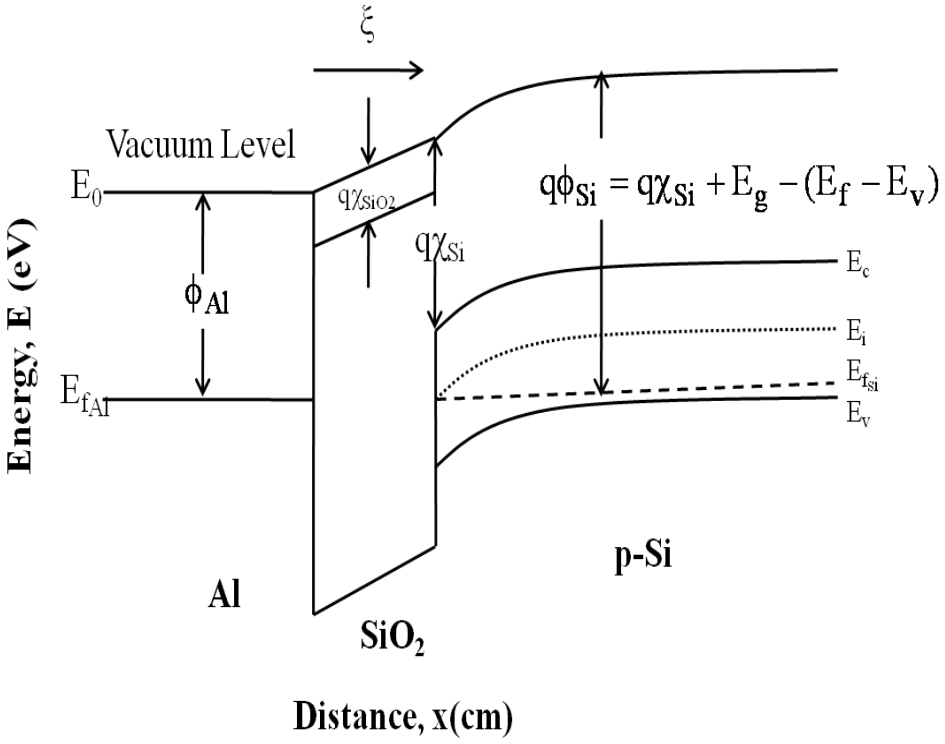

Fig. 8. Energy band diagram of ideal MOS capacitor

band voltage and is represented by V_{FB}^0 for an ideal MOS capacitor. The expression for the ideal flat-band voltage from [12] is given below

$$V_{FB}^{0} = \phi_m - \phi_s = \{\phi_m - \frac{q\chi_{Si} + E_g - (E_f - E_v)}{q}\}, \qquad (4.2)$$

where ϕ_m is the metal work function, ϕ_s is the semiconductor work function, q is the electronic charge, E_g is the band gap of silicon, E_f and E_v are the Fermi level and valence band energy level of silicon respectively.

4.4 Ideal MOS capacitor threshold voltage

The potential and the spatial coordinate system are defined in Fig. 9. The zero potential is chosen to be the semiconductor intrinsic energy level E_i. The potential or voltage anywhere in the semiconductor is measured from the bulk zero reference. At the surface of the semiconductor it is called surface potential and it is the total voltage drop across the semiconductor, measured from the surface to the bulk reference.

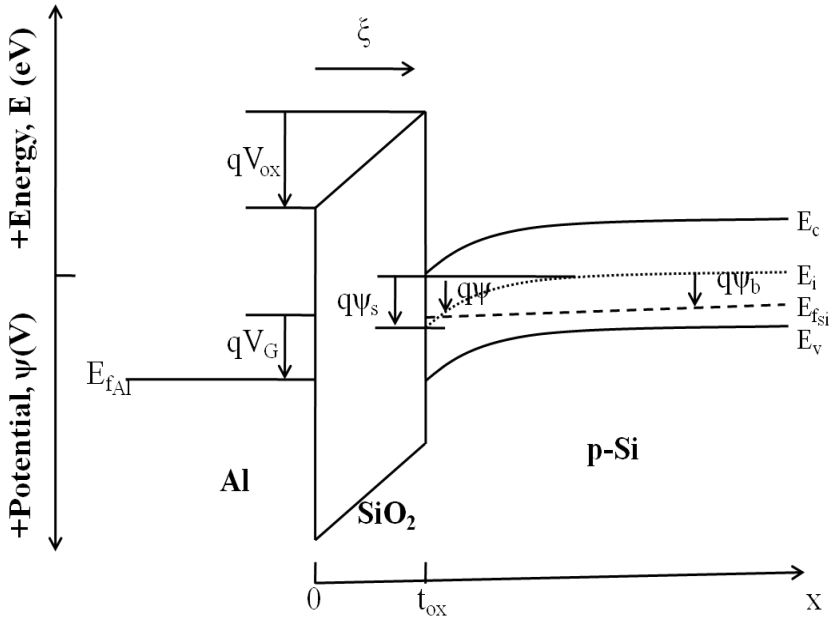

Fig. 9. Energy band diagram of MOS capacitor showing potentials and spatial dimension

The bulk potential ψ_b and the surface potential ψ_s are given as,

$$\psi_b = (E_i(\text{bulk}) - E_f)/q \quad , \tag{4.3}$$

$$\psi_s = (E_i(\text{bulk}) - E_i(x = t_{ox}))/q \, , \tag{4.4}$$

where E_i(bulk) is the intrinsic energy level in the bulk of the semiconductor, $E_i(x=t_{ox})$ is the intrinsic energy level at the semiconductor surface. For a p-type Al/SiO_2/p-Si MOS capacitor, a positive gate bias has to be applied in order to invert the semiconductor surface. The gate voltage V_G applied to the MOS capacitor is given as,

$$V_G = V_{FB}^0 + V_{ox} + \psi_s \, , \tag{4.5}$$

where V_{ox} is the voltage drop across the oxide and ψ_s is the surface potential. Gauss's law can be used to estimate the voltage drop across the gate oxide V_{ox}. From Gauss's law the surface integral of electric flux density is equal to charge enclosed and is given by

$$Q = \varepsilon \oint \xi da \, , \tag{4.6}$$

where Q is the charge, ε is the permittivity, ξ is the electric field. From the integral in Equation 4.6,

$$Q_{sc} = -\varepsilon_{ox} \xi_{ox} A \, , \tag{4.7}$$

where ε_{ox} is the permittivity of silicon dioxide, ξ_{ox} is the electric field across the oxide and A is the cross-sectional area of the MOS capacitor. The electric field in the oxide is given as

$$\xi_{ox} = -\frac{Q_{sc}}{\varepsilon_{ox} A} \, . \tag{4.8}$$

The space charge in the semiconductor Q_{sc} is given as

$$Q_{sc} = -A\sqrt{4q\varepsilon_{Si} N_a^- |\psi_b|}, \tag{4.9}$$

where ε_{Si} is the permittivity of silicon, N_a^- is the ionized acceptor impurity concentration. At the Si/SiO_2 interface, the electric flux density has to be continuous and this gives

$$D_{ox} = D_{Si} \xrightarrow{\text{yields}} \varepsilon_{ox}\xi_{ox} = \varepsilon_{Si}\xi_{Si} \ . \tag{4.10}$$

D_{ox} and D_{Si} are the electric flux density on the oxide and semiconductor sides respectively. The potential ψ_{ox} is the integration of the electric field and is given as

$$\psi_{ox}(x) = -\int \xi_{ox} dx \quad . \tag{4.11}$$

Evaluating the above integral and substituting the boundary condition $\psi(t_{ox}) = \psi_s$ gives

$$\psi_{ox}(x) = \psi_s + \xi_{ox} t_{ox} - \xi_{ox} x \ \text{ for } 0 < \ x < t_{ox}, \tag{4.12}$$

where ψ_s is the surface potential in semiconductor, t_{ox} is the thickness of oxide. The potential across the oxide V_{ox} is the difference in the potential at x=0 and $x=t_{ox}$

$$V_{ox} = \psi_{ox}(0) - \psi_{ox}(t_{ox}) = \xi_{ox} t_{ox} . \tag{4.13}$$

By substituting for ξ_{ox} from Equation 4.8 and Q_{sc} from Equation 4.9, the above expression becomes

$$V_{ox} = \frac{t_{ox}\sqrt{4qN_a^- t_{ox}\varepsilon_{Si} |\psi_b|}}{\varepsilon_{ox}} . \tag{4.14}$$

The ideal threshold voltage of the MOS capacitor is given as

$$V_T = V_G = \psi_t + V_{ox} + V_{FB}^0, \tag{4.15}$$

where V_T is the threshold voltage of the MOS capacitor, V_G is the applied gate voltage and ψ_t is the surface potential at threshold voltage. By using $\psi_t = 2|\psi_b|$ and substituting V_{ox} from Equation 4.14, the threshold voltage of the p-type MOS capacitor is given as

$$V_T = V_{FB}^0 + 2|\psi_b| + \frac{\sqrt{4q|\psi_b|\varepsilon_{Si}N_a^-}}{\varepsilon_{ox}/t_{ox}} \ . \tag{4.16}$$

4.5 MOS capacitance – voltage behavior

The MOS system consists of a series combination of oxide capacitance C_{ox} and semiconductor capacitance C_{Si}. Fig. 10 is a schematic representation of the MOS capacitor.

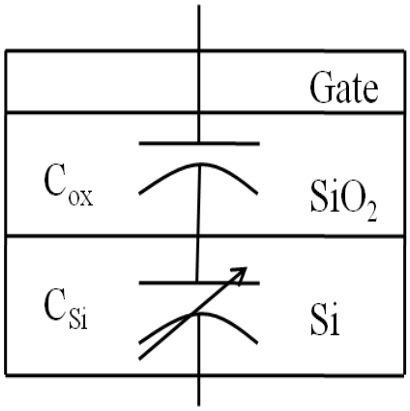

Fig. 10. Schematic representation of MOS capacitor

The gate to bulk voltage applied to the MOS capacitor is given by

$$V_{GB} = V_{FB}^0 - \frac{Q_{Si}^{'}}{\varepsilon_{ox}} t_{ox} + \psi_s, \tag{4.17}$$

where V_{GB} is the gate to bulk voltage, Q'_{Si} is the semiconductor charge per unit area. The total capacitance of the MOS capacitor is given as

$$\frac{1}{C'_{dif}} = \frac{1}{C'_{ox}} + \frac{1}{C'_{Si}}, \tag{4.18}$$

where C'_{dif} is the differential capacitance per unit area of the MOS capacitor, C'_{ox} and C'_{Si} are the oxide and silicon capacitance per unit area respectively. The semiconductor charge per unit area is given as

$$Q'_{Si} = \sqrt{2qN_a^- \varepsilon_{Si}} \sqrt{\phi_t e^{\frac{-\psi_s}{\phi_t}} + \psi_s - \phi_t + e^{\frac{-2\psi_b}{\phi_t}} (\phi_t e^{\frac{\psi_s}{\phi_t}} - \psi_s - \phi_t)}, \tag{4.19}$$

where ϕ_t is the thermal voltage, ψ_s and ψ_b are given by Equations 4.3 and 4.4. The thermal voltage is given as $\phi_t = \frac{kT}{q}$, where k is Boltzmann constant, T is the temperature. When the semiconductor is in accumulation region i.e $|\psi_s| > 3\phi_t$, then the differential capacitance C_{dif}' (acc) is approximately equal to oxide capacitance.

$$C'_{dif}(acc) = C'_{ox}(F/cm^2). \tag{4.20}$$

The flat band capacitance C_{dif}' (FB) corresponds to the value when the bands are flat and is given by the equation

$$C'_{dif}(FB) = \frac{1}{\frac{t_{ox}}{\varepsilon_{ox}} + \frac{L_D}{\varepsilon_{Si}}}(F/cm^2), \tag{4.21}$$

where $L_D = \sqrt{\frac{\varepsilon_{Si} kT}{q^2 N_a^-}}$ is the Debye length, ε_{Si} is the permittivity of silicon, k is Boltzmann constant, T is the temperature. The inversion capacitance C_{dif}' (inv) corresponds to the value when $\psi_s = 2|\psi_b|$ and there is maximum depletion in the semiconductor region. The capacitance is given by the equation

$$C'_{dif}(\text{inv}) = \frac{1}{\frac{t_{ox}}{\varepsilon_{ox}} + \frac{x_{d_{max}}}{\varepsilon_{Si}}} (F/cm^2) \ . \qquad (4.22)$$

Fig. 11 is the comparison of normalized C-V curve calculated using the analytical equations 4.12-4.14 and experimental data. The figure shows that the ideal equation does not match with experimental data. This is due to non-idealities in the oxide which introduce traps near the interface which when occupied causes deviation from the ideal behavior.

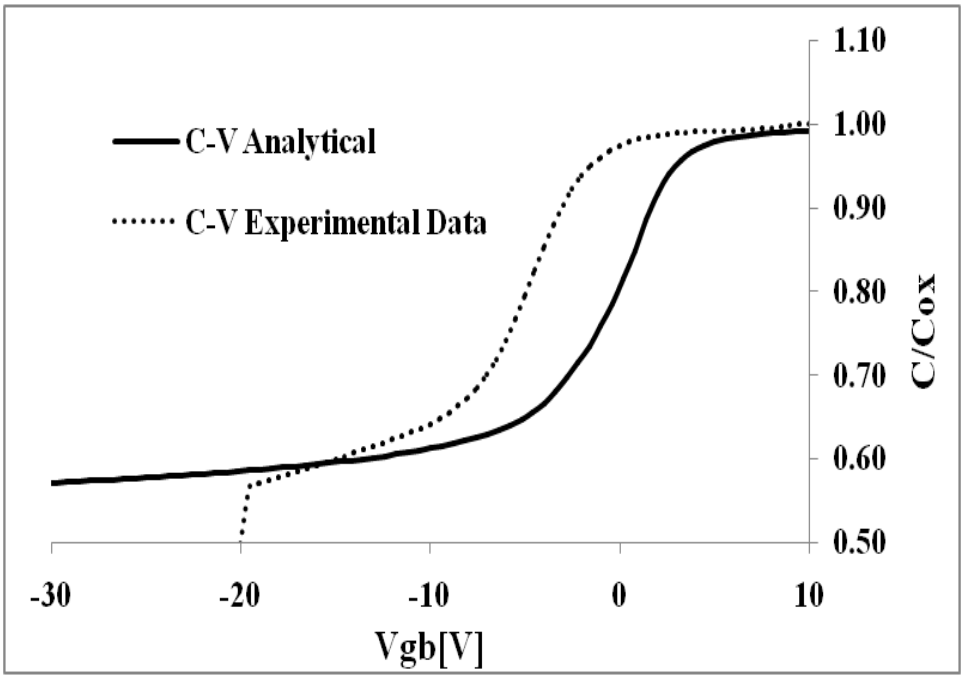

Fig. 11. Comparison of ideal MOS C-V curve with experimental data

4.6 Non-ideal capacitance – voltage Behavior

4.6.1 Fixed oxide charge- Q_f

The oxide is not ideal and typically has some fixed charge which is likely to have been introduced during the oxide growth. The fixed oxide charge Q_f is very near the silicon/insulator interface and this changes the flat-band voltage to $V_{FB} = V_{FB}^0 - \frac{Q_f}{\varepsilon_{ox}/t_{ox}}$. The gate to bulk voltage of the MOS capacitor becomes

$$V_{GB} = V_{FB}^0 - \frac{Q_f}{\varepsilon_{ox}/t_{ox}} + \frac{t_{ox}Q_{Si}^{'}}{\varepsilon_{ox}} + \psi_s . \qquad (4.23)$$

From the above equation it can be seen that the gate voltage required to measure the same effective capacitance is shifted by $\frac{t_{ox}Q_f}{\varepsilon_{ox}}$. This shift depends on the polarity of the charge and can shift the C-V curve to the left or right.

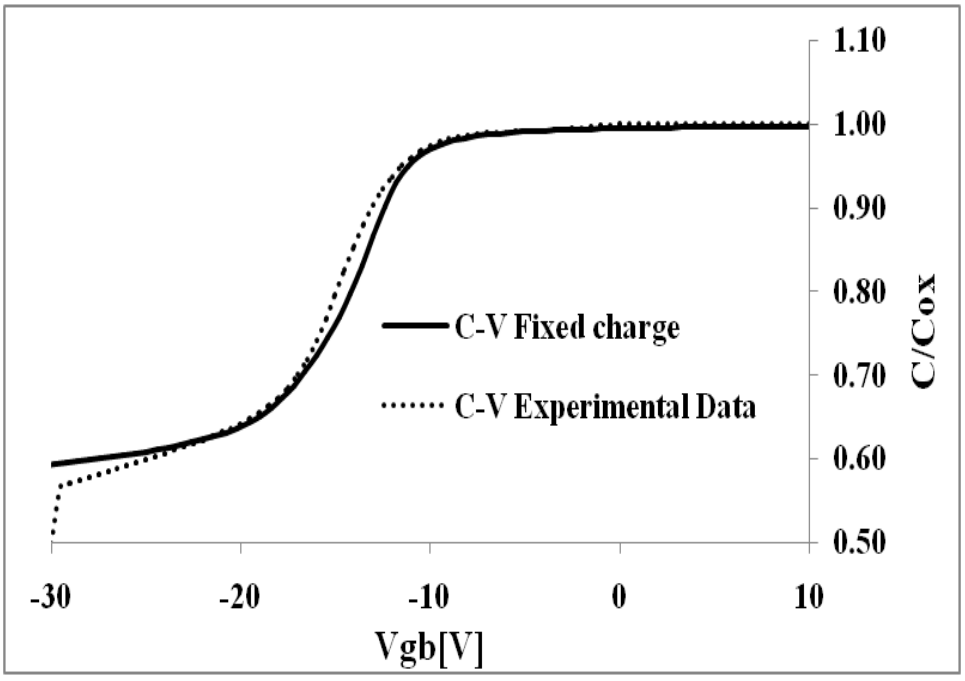

Fig. 12. Comparison of experimental data with non ideal MOS C-V curve

Shown in Fig. 12 is the comparison of C-V curve obtained using the analytical equation including the impact of fixed oxide charge and experimental data. It can be seen that the experimental data match very well with the analytical model.

4.6.2 Interface trap charge- Q_{it}

Another non-ideality is introduced because of dangling bonds in the silicon/insulator interface. These dangling bonds introduce energy levels distributed throughout the forbidden band gap which are called surface states or interface states [12] shown in Fig. 13(a). Fig. 13(b) represents an n-type MOS capacitor biased in inversion and the Fermi level at the surface lies close to E_v. All energy levels below the Fermi level are filled with electrons while all energy levels above are empty. So in case (b) no interface state if filled and assuming that the interface states are donor-like in nature, the net charge per unit area Q_{IT} will be positive. In Fig. 13(c) the MOS capacitor is biased in accumulation and it can be seen that all the interface states are occupied by electrons. If all the donor-like interface states are occupied by electron then there is no contribution of interface trap charge. The interface trap charge contribution depends on the bias condition of the MOS capacitor. The shift in the gate to bulk voltage due to interface trap charge is given as

$$\Delta V_{GB} = -\frac{Q_{IT}}{C_{ox}}, \tag{4.24}$$

where Q_{IT} is the net contribution of interface trap charge and C_{ox} is the oxide capacitance per unit area.

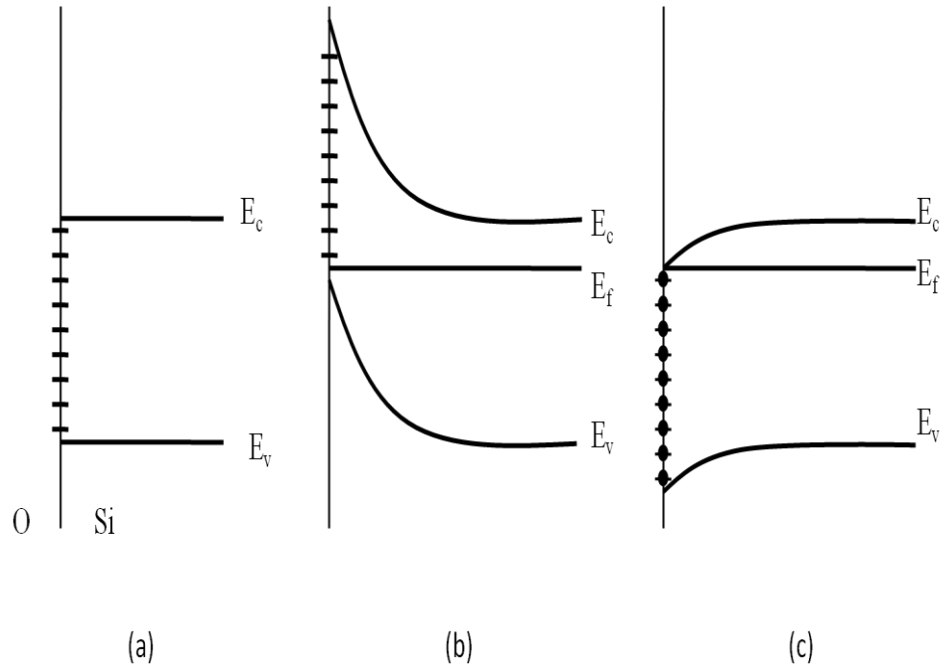

Fig. 13. Illustration of interface states at different biasing conditions in an MOS capacitor

4.7 Extraction of oxide-trapped charge and interface trap charge from C-V curve

In order to extract the oxide-trapped charge N_{OT} and interface traps, N_{IT}, the technique described from [13] is used. Flat-band, midgap and strong inversion capacitance are identified and these correspond to a surface potential ψ_s of 0, ϕ_b and $2\phi_b$. The total voltage shift is given as

$$\Delta V_{total} = \Delta V_{N_{OT}} + \Delta V_{N_{IT}}, \tag{4.25}$$

where $\Delta V_{N_{OT}}$ is the net voltage shift due to oxide-trapped charge Q_{OT} and $\Delta V_{N_{IT}}$ is the net voltage shift due to interface trap charge Q_{IT} .The assumption made for the extraction is that the interface states in the upper half of the band gap are acceptor like and those in the lower half are donor like. The total voltage shift at midgap gives $\Delta V_{N_{OT}}$ since at midgap there is no charge contribution from the

interface states. The voltage stretch out from midgap to inversion gives $\Delta V_{N_{IT}}$, which is the shift due to the occupied interface states between midgap and inversion.

Chapter 5

THE DOSE PERFORMANCE OF THE RADCAP

5.1 Processing technique

5.1.1 Wet oxidation and dry oxidation

Thermal oxidation is a way to grow a layer of silicon dioxide of desired thickness on the surface of a semiconductor wafer. An oxidizing agent diffuses into the wafer at high temperatures and results in the formation of silicon dioxide, thereby determining the rate of growth of oxide. Thermal oxidation is performed at a temperature of around 800°C to 1200°C using two different oxidizing agents. Wet oxidation uses water vapor as the oxidizing agent while molecular oxygen is used for dry oxidation. The oxidizing ambient also contains several percent of hydrogen chloride which is used to remove the metal ions from the oxide. The reaction for oxidation, wet and dry respectively, is as follows

$$Si + 2H_2O \rightarrow SiO_2 + 2H_2 \tag{5.1}$$

and

$$Si + O_2 \rightarrow SiO_2. \tag{5.2}$$

The Si in the above reaction is supplied by the substrate while the oxygen or water vapor is available from the ambient. The main difference between the above reactions is the oxide growth rate. Dry oxidation is preferred over wet oxidation for thinner oxides (<100 nm). This is due the fact that it introduces less water molecules inside the oxide. Since wet oxidation has faster growth rate it is usually preferred over dry oxides for thicker oxides (>200 nm). The drawback of wet oxidation is that it leaves dangling bonds at the interface and results in low

density oxides [8]. Mobile ions (sodium) can degrade the performance of MOS capacitors and to immobilize them hydrogen chloride or trichloroethylene is introduced. They also tend to increase the rate of oxidation thereby forming a positive feedback for oxidation.

For the works, RADCAPs were prepared by growing oxides using dry oxidation and wet oxidation to see their impact on the dose response. An earlier work [14] suggested that the mechanism involved in the interface state development is the same but the magnitude is much smaller in thermally grown dry oxides as compared to wet oxides. The difference is primarily due to the different amounts of water incorporated in the oxide during processing. Since the water related species is primarily responsible for the interface trap buildup, a difference in processing will have a huge impact on the dose response of the sample. The reaction from [14] is as follows

$$H_2O + DB \rightarrow SiOH + H, \tag{5.3}$$

$$H_2O + DB \rightarrow SiH + OH, \tag{5.4}$$

where DB is the dangling Si bond and OH is the interstitial species. These reactions suggest that the water molecules may passivate a bare dangling bond and release an H or OH atom. Both of the above mentioned reactions are feasible at room temperature. The mechanism for interface trap buildup involves protons moving under the influence of a positive gate bias towards the interface where they break a Si-OH or Si-H bond to leave behind a dangling Si- bond that forms the interface trap [15].

5.1.1.1 Experiment results

RADCAP samples with two different oxide thicknesses – 100 nm and 200 nm were prepared for an experimental assessment of the impact of oxide processing on dose response. Dry oxidation was used to grow oxide on the 100 nm samples while wet oxidation was used for 200 nm samples. These capacitors were irradiated with ^{60}Co irradiations under a gate bias of 5V and their corresponding C-V curves were recorded at different dose levels of 20 krad, 100 krad and 279 krad. In order to make sure that there is no sample to sample variation, C-V curves were recorded on 14 samples in total (7 with 100 nm oxide thickness and 7 with 200 nm oxide thickness). In order to eliminate the parasitic capacitance introduced by the measurement setup, the capacitance was normalized with respect to its accumulation capacitance value (C_{accum}). The normalized C-V curves of the 100 nm and 200 nm samples are shown in Figs. 14 and 15 respectively. It can be seen from C-V curves that the RADCAPs with 200 nm oxide thickness show more interface states than their 100 nm counterparts at higher dose levels.

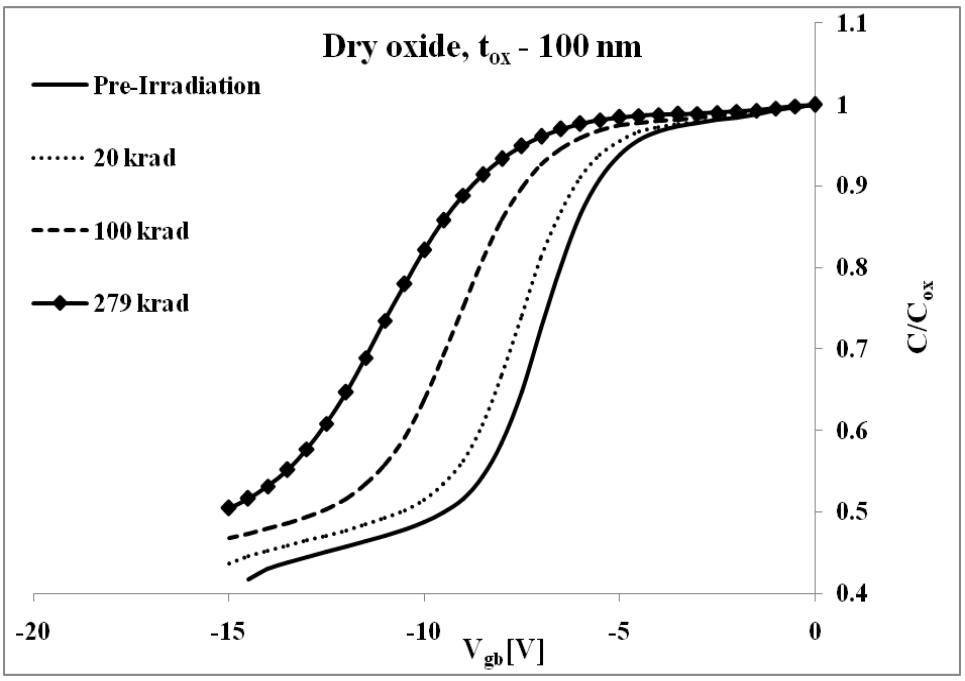

Fig. 14. Pre-irradiation and post-irradiation C-V curves of RADCAP with 100 nm (dry) oxide thickness

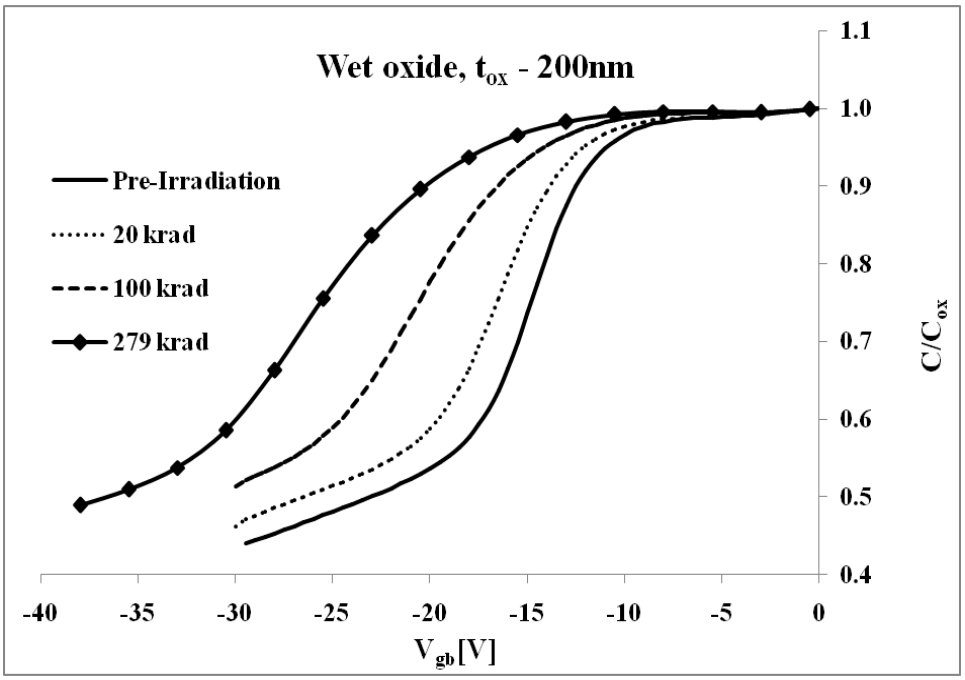

Fig. 15. Pre-irradiation and post-irradiation C-V curves of RADCAP with 200 nm (wet) oxide thickness

The buildup of oxide-trapped charge as a function of radiation dose level is given by

$$\Delta N_{OT} = g_0 t_{ox} f_y(E_{ox}) D, \tag{5.5}$$

where g_0 is the initial electron-hole pair volume density, t_{ox} is the oxide thickness, $f_y(E_{ox})$ is the fractional hole yield and D is the total radiation dose. The change in oxide-trapped charge ΔN_{OT} and interface trap density ΔN_{IT} was extracted from experimental data to estimate the dose sensitivity. These values were normalized with respect to oxide thickness and fractional hole yield in order to provide a fair comparison of the processing scheme. Figs. 16 and 17 show the normalized oxide-trapped charge and interface trap density of RADCAPs with 100 nm and 200 nm oxide thickness.

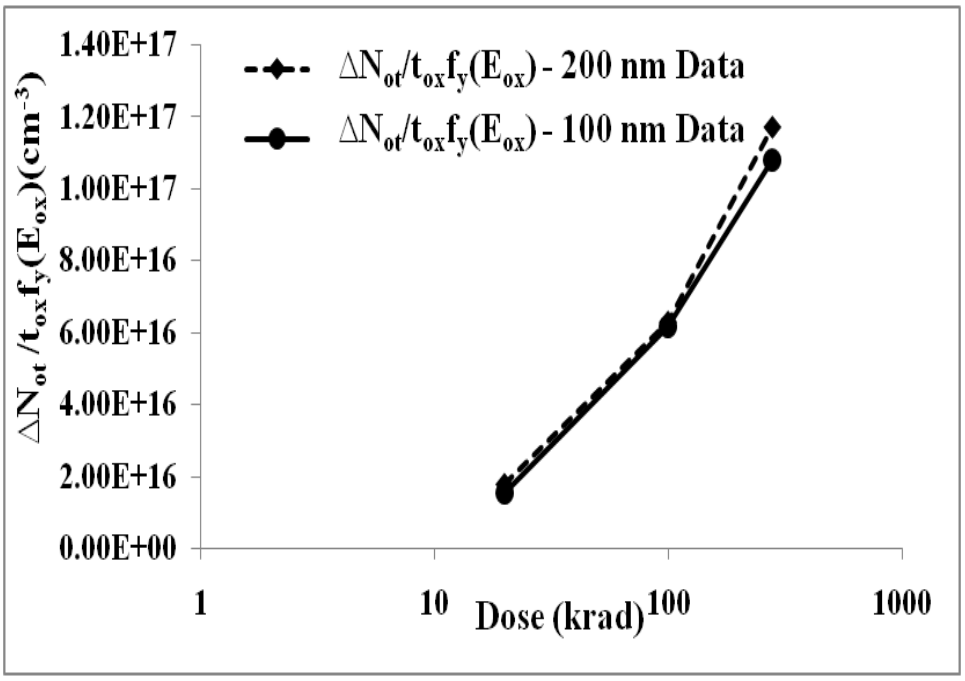

Fig. 16. Experimental data of normalized oxide-trapped charge density of RADCAP with 100 nm (dry) and 200 nm (wet) oxide thickness

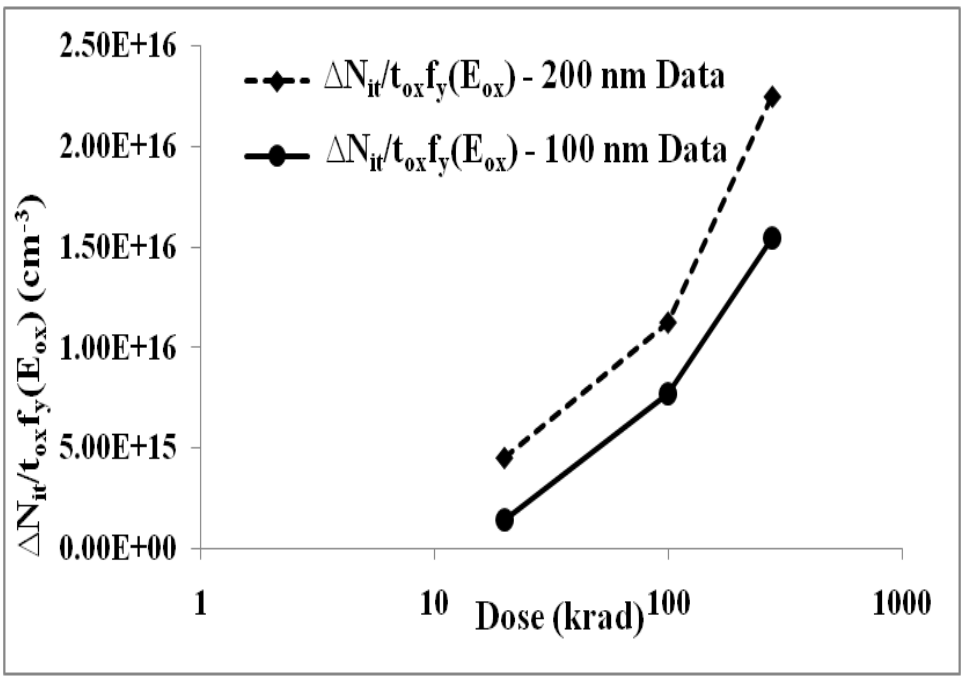

Fig. 17. Experimental data of normalized interface trap density of RADCAP with 100 nm (dry) and 200 nm (wet) oxide thickness

The normalized oxide-trapped charge density is nearly the same in both the samples indicating that the number of hole trapping precursor sites is very similar. The 100 nm samples show lower interface trap density than the 200 nm samples, but not a large difference. The small difference is most likely due to the presence of H species in the wet oxidized samples which are responsible for the interface state charge [17-20]. Interface traps impact the shape of the C-V curve and degrade the performance of the dose sensor thus the dry oxidized RADCAP is somewhat better for dosimetry.

The initial precursor hole trap density in both oxides can be estimated using Radiation Effects Module (REM) present in Silvaco device simulator. MOS capacitors with similar oxide thicknesses as the experimental samples were used in the simulation. The initial precursor hole trap density was 10^{18} cm^{-3} for both

samples with 100 nm and 200 nm oxide thicknesses. Figs. 18 and 19 compare the change in oxide-trapped charge ΔN_{OT} estimated using simulation against experimental data for samples having oxide thickness of 100 nm and 200 nm. As can be seen, the simulation data match very well with the experimental data indicating that the initial precursor hole trap density extracted using simulations is close to the experimental value.

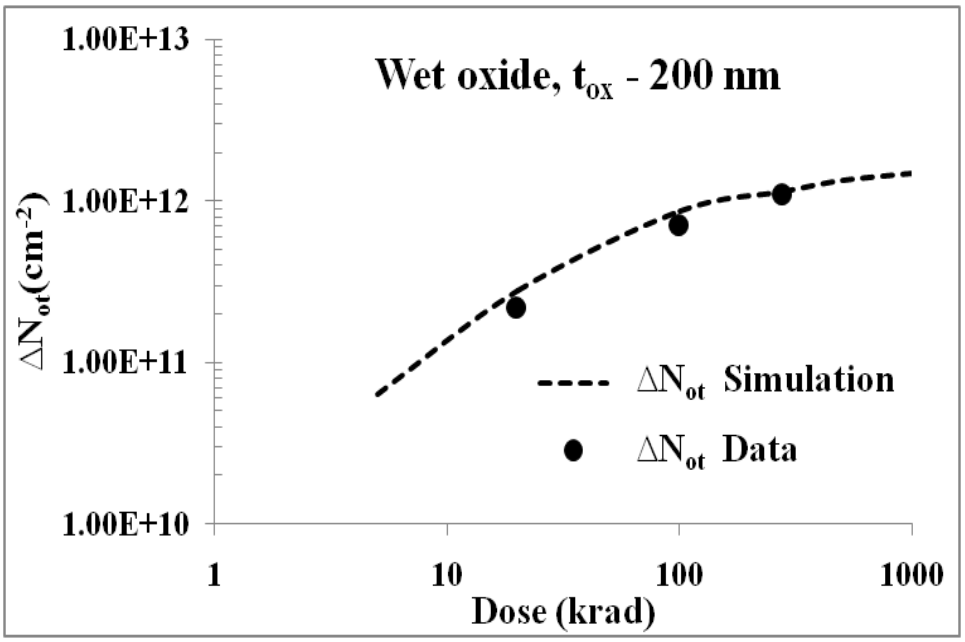

Fig. 18. Comparison of oxide-trapped charge per unit area for RADCAP with 200 nm oxide thickness (wet) obtained from simulation and experimental data

In order to further validate the simulation results, C-V curves were simulated for the 100 nm and 200 nm oxide samples with the ΔN_{OT} values extracted from simulation. The midgap voltage shifts obtained from simulation were compared against experimental data. Figs. 20 and 21 compare the midgap voltage as function of dose obtained using simulation and experiments for samples with 100 nm and 200 nm oxide thickness. The simulations match very

well with experimental data validating the accuracy of the selected precursor density estimated using simulations.

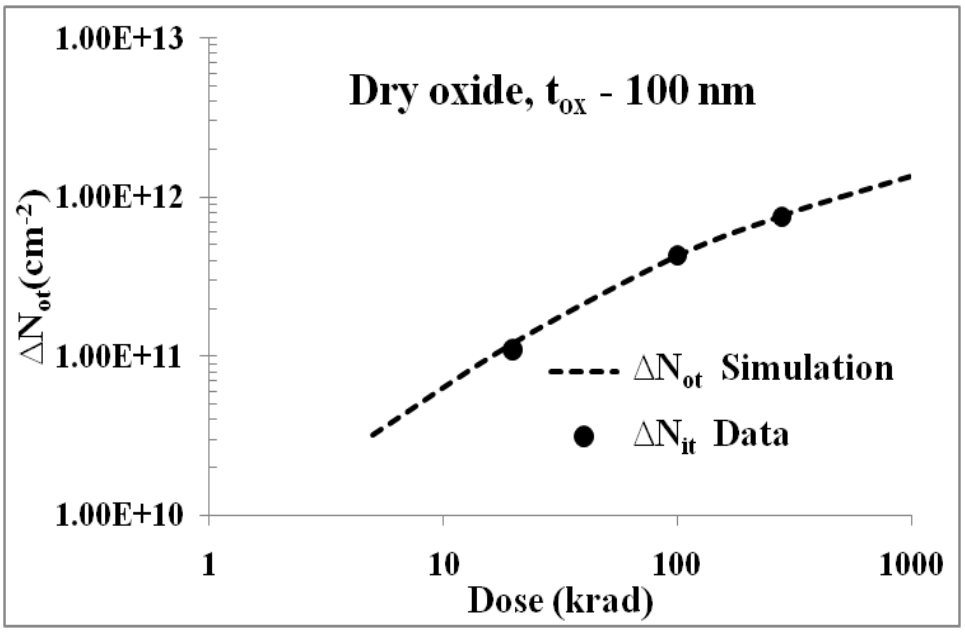

Fig. 19. Comparison of oxide-trapped charge per unit area for RADCAP with 100 nm oxide thickness (dry) obtained from simulation and experimental data

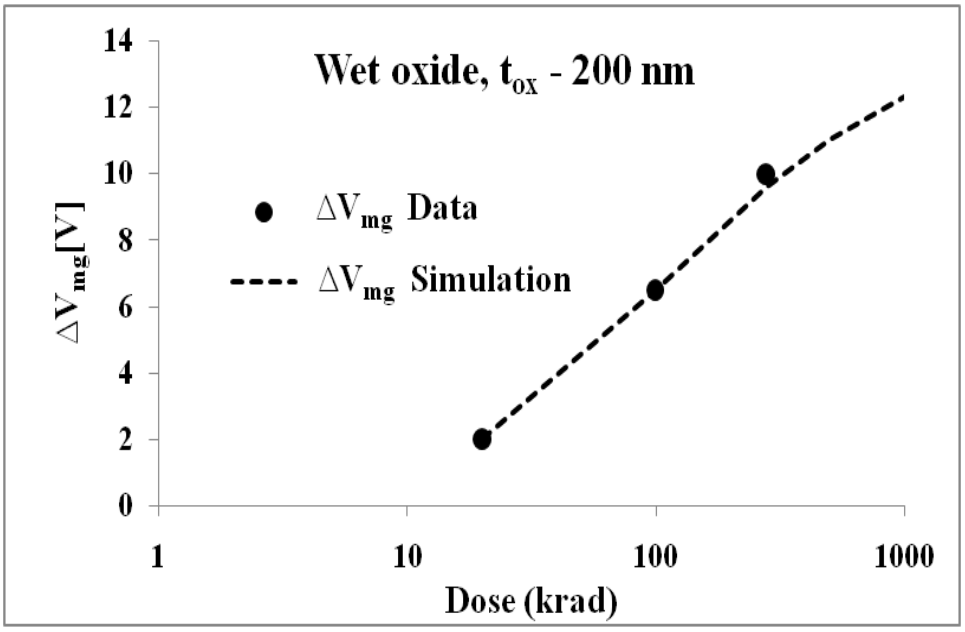

Fig. 20. Comparison of midgap voltage shifts for RADCAP with 200 nm oxide thickness (wet) obtained from simulation and experimental data

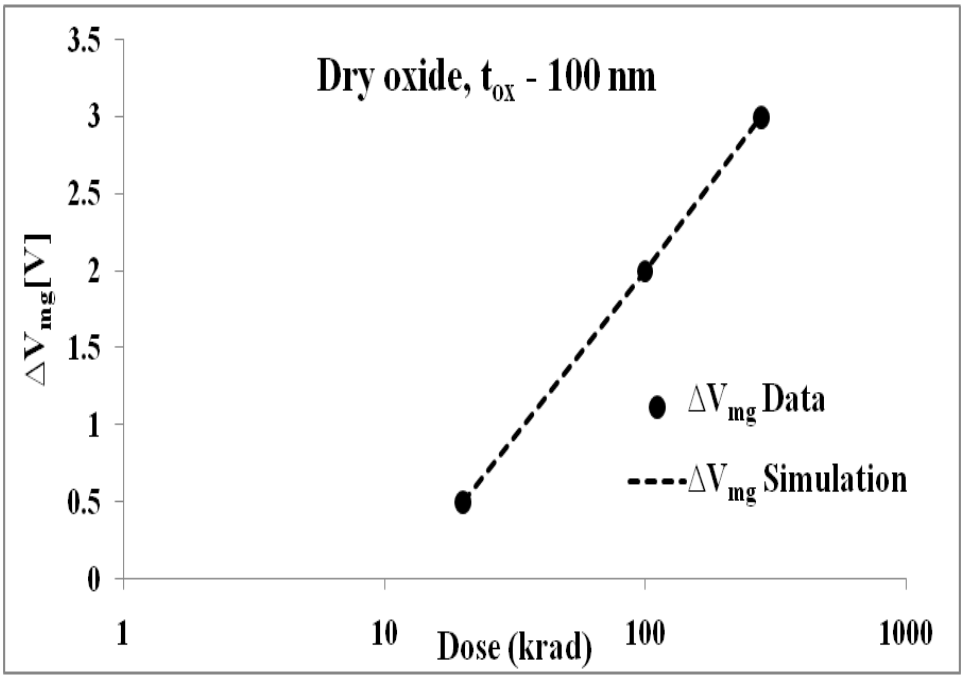

Fig. 21. Comparison of midgap voltage shifts for RADCAP with 100 nm oxide thickness (dry) obtained from simulation and experimental data

5.1.2 Thermally grown high quality oxide

5.1.2.1 Fabrication steps

In order to study the dose sensitivity of a thermally grown high quality oxide, RADCAPs were manufactured using p-type SOI wafers. SOI wafers were chosen so that the device silicon layer can be kept very thin thereby reducing the series resistance. This type of process is ideal for the proposed capacitively-loaded wireless sensor application described earlier. The oxide in these wafers was 2 µm thick. The fabrication steps are summarized in Fig. 22. The first step is to deposit silicon nitride on both sides of the wafer using Low Pressure Chemical Vapor Deposition (LPCVD). In order to form the capacitor the silicon underneath

the silicon dioxide layer has to be etched. A photo resist is patterned on the backside of the wafer to enable removal of the silicon nitride layer.

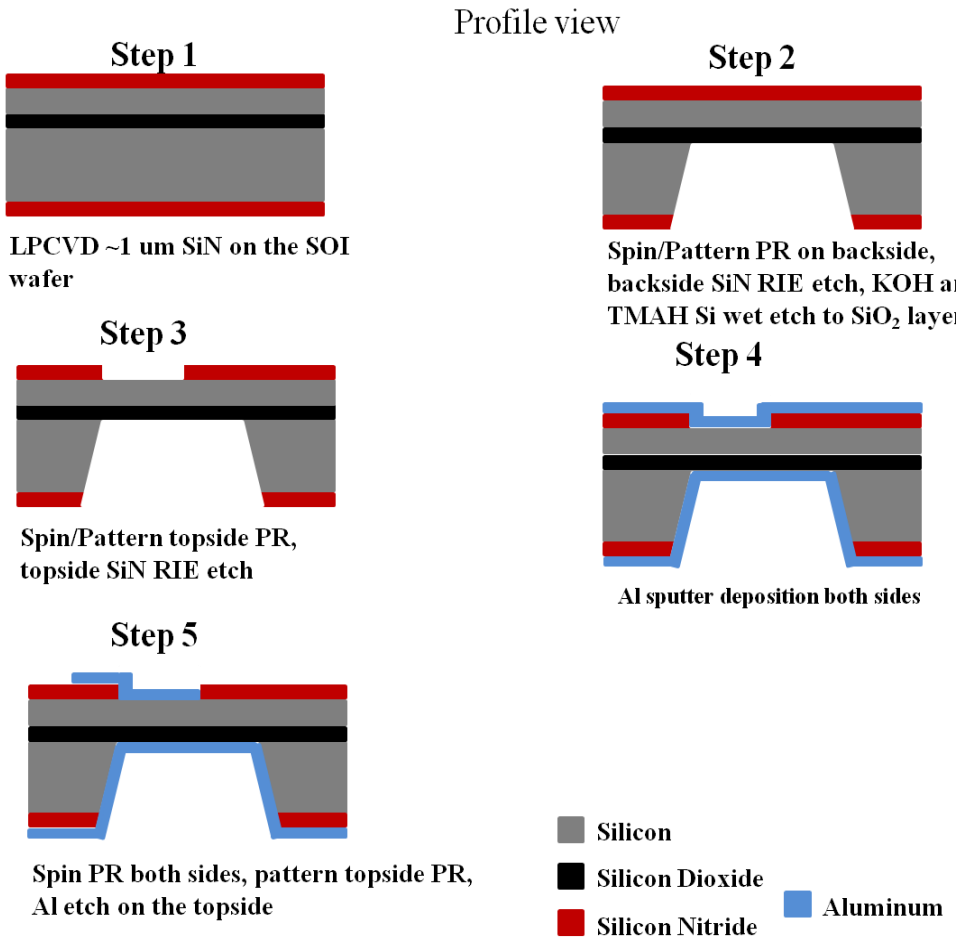

Fig. 22. Fabrication steps to manufature capacitors using SOI wafers

Step 2 consists of Reactive Ion Etch (RIE) using potassium hydroxide (KOH) to remove backside silicon layer. KOH etch is used to remove most of the silicon far away from the oxide layer. Since KOH aggressively attacks the oxide causing reductions in its thickness, silicon wet etch (TMAH) is used to remove the silicon close to the oxide layer. In step 3, a photo resist pattern is used on the top side to enable removing silicon nitride using reactive ion etch. Aluminum contacts are

formed on both sides of the capacitor by sputtering and this forms step 4. In order to remove the unwanted aluminum from other portions of the wafer, a photo resist is patterned on the top side which forms step 5. After etching out the aluminum, Post Metallization Annealing (PMA) is done in the presence of nitrogen for 10 minutes.

5.1.2.2 Experiment results

The capacitors manufactured using the fabrication steps described above was exposed to a 700 keV proton beam to study their dose response and performance as dose sensor. The flux rate of the ion beam was $3.98 \times 10^{10} cm^{-2} sec^{-1}$. As these capacitors are expected to be used as passive dose sensors no bias was applied while exposing them to the proton beam.

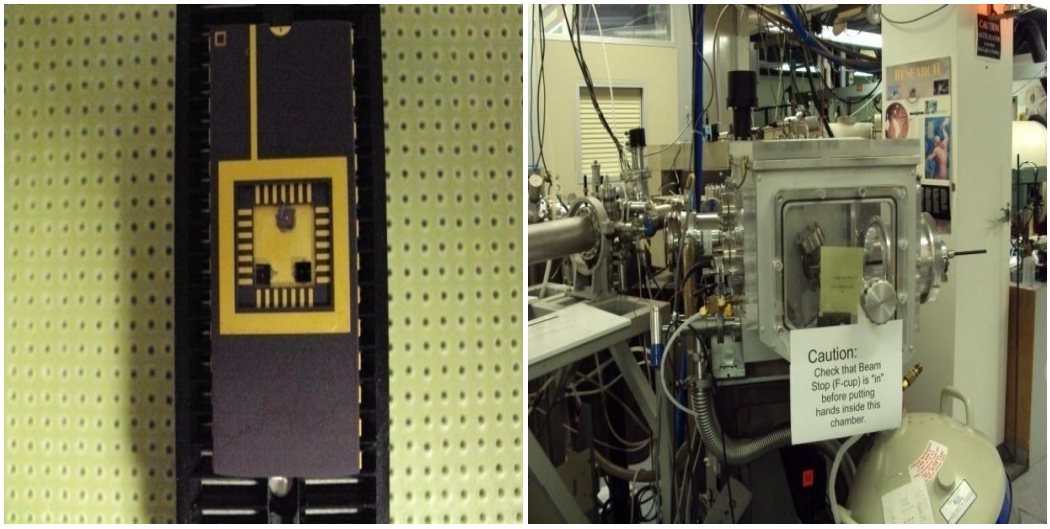

Fig. 23. Package containing RADCAPs with high quality oxide and the proton beam chamber used for irradiation

Fig. 23 shows photographs of the packaged capacitor and the radiation chamber used to irradiate the parts. Under the irradiation condition the charge yield is very

low and most of the electron hole pairs created is lost to geminate recombination [11].

Fig. 24 shows the results of the proton beam irradiation. The capacitors show a left shift as a result of oxide-trapped charge and this shift increases as a function of dose.

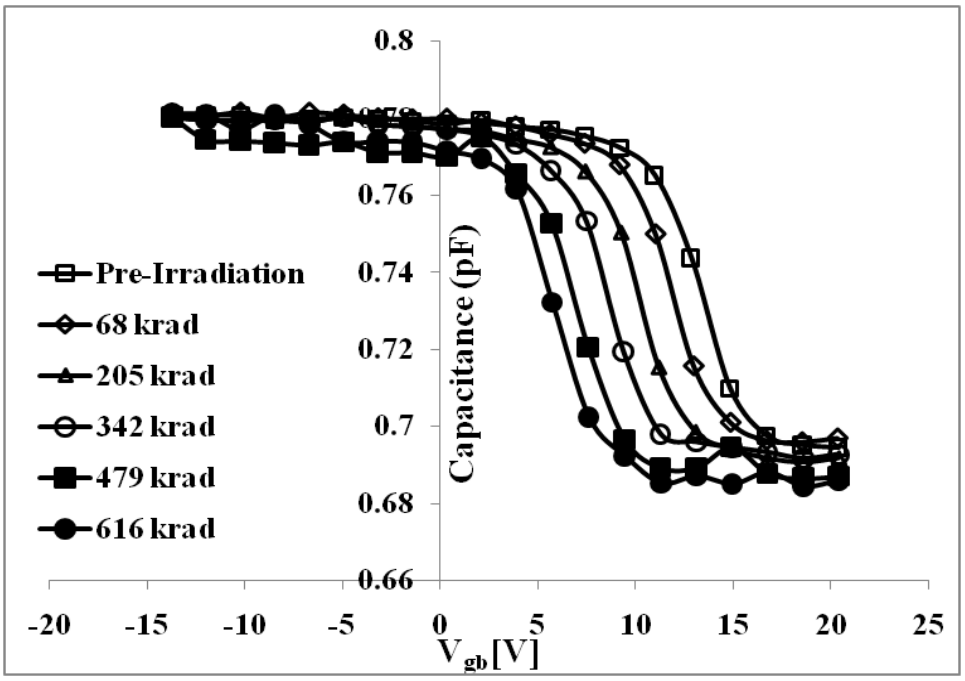

Fig. 24. Experimental data showing radiation response of RADCAP with high quality oxide

Even though the charge yield is low for 700 keV proton beam [11] substantial voltage shifts can be seen in the data indicating the radiation sensitivity of these capacitors. Fig. 25 shows capacitance as a function of dose at a gate to body bias of 8V. It can be seen that the capacitance changes as a function of dose which can be used in the system design described in section 4.2. This change of capacitance gives a difference in the resonant frequency that can be mapped back to find the dose level.

There are various parameters that control the dose sensitivity and dynamic range of the sensor. The above described sensor has a dynamic range of 600 krad for the proton beam.

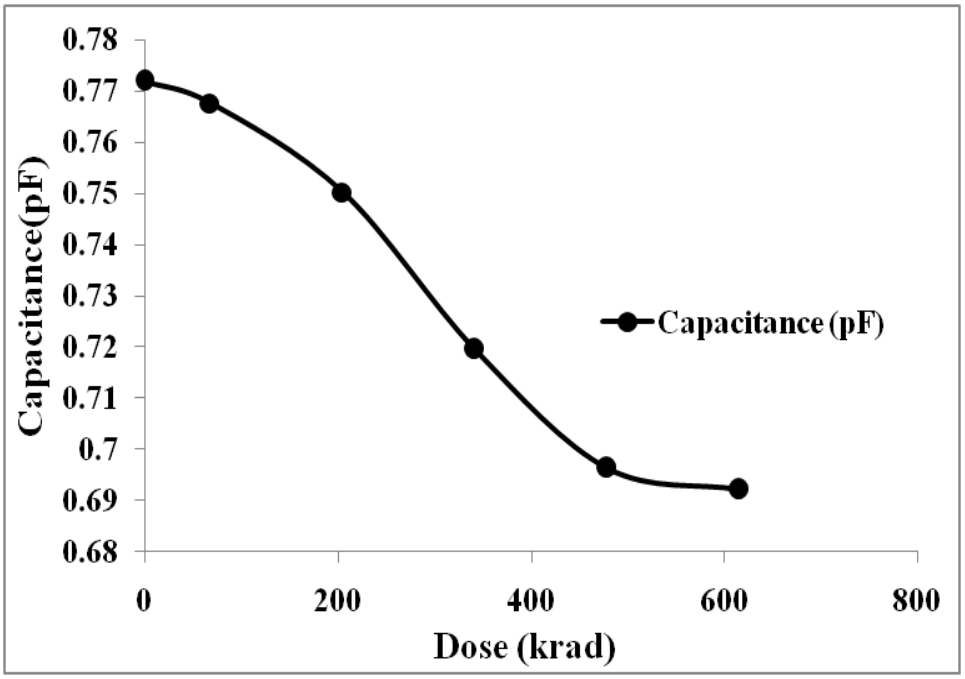

Fig. 25. Capacitance versus dose map for RADCAP with high quality oxide

For the system described in section 4.2, the capacitance at zero bias must change as a function of dose. From Fig. 24 it can be seen that, at zero bias there is no change in capacitance due to ionizing radiation. This is due to the fact that the threshold voltage prior to irradiation is too high. In order to shift the C-V curves in Fig. 24 to the left, the doping of the device silicon in the SOI wafer can be reduced thereby resulting is lower threshold voltage.

In order to quantatively analyze the effectiveness of the dose senor, the change in oxide-trapped charge ΔN_{OT} was extracted from the experimental data. The initial precursor hole trap density in the oxide estimated using the REM

module of Silvaco device simulator is 1.5×10^{16}cm^{-3}. Fig. 26 shows the comparison of oxide-trapped charge as a function of dose estimated using simulation against experimental data. It can be seen from Fig. 26 that the change in oxide-trapped charge, ΔN_{OT}, begins to saturate at higher doses indicating that most of the trapping sites have been filled with holes. This sets a limit on the dynamic range of doses this capacitor can be used as a dose sensor. The data also show no interface traps indicating that with proper control, thermal oxidation can yield high quality oxides that can be used as better dose sensors.

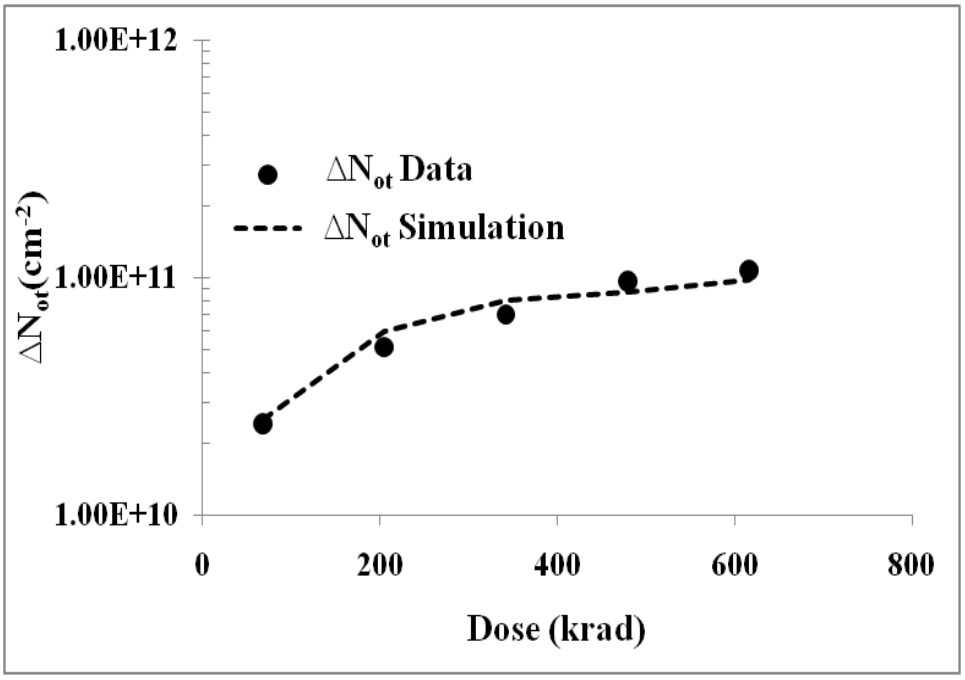

Fig. 26. Comparison of oxide-trapped charge per unit area for RADCAP with high quality oxide obtained from simulation and experimental data

5.2 Dielectric material

In order to study further the effects of different dielectric materials, RADCAPs with silicon nitride and silicon dioxide as gate insulators were

manufactured. Silicon dioxide capacitors were prepared using the dry oxidation technique described in section 5.1. Silicon nitride was deposited on silicon using Low Pressure Chemical Vapor Deposition (LPCVD). Silicon nitride dielectrics deposited using LPCVD had up to 8% hydrogen in them. These capacitors along with other oxide samples were packaged and exposed to ^{60}Co radiations. Their C-V curves were recorded at dose levels of 20 krad, 100 krad and 279 krad. The electron hole pair generation in the dielectric is controlled by the following equation

$$\frac{\#\text{ehp}}{\text{cm}^3\text{s}} = \text{LET} \times \rho \times \frac{1}{E_p} \times \phi_f \,, \tag{5.6}$$

where ρ is the density of silicon nitride, ϕ_f is the flux, and E_p is the energy needed to produce an electron hole pair in nitride. Table 3 from [21] provides a comparison of properties of silicon nitride and silicon dioxide.

PARAMETER	**Silicon Nitride**	**Silicon dioxide**
E_p	10.8 eV/ehp	17.4 eV/ehp
LET (^{60}Co-700 kev)	2.457 MeV/(mg/cm^2)	2.171 MeV/(mg/cm^2)
ρ	3.1 g/cm^3	2.2 g/cm^3

Table 3. Comparison of properties of silicon nitride and silicon dioxide

Comparing the above quantities, silicon nitride samples have 2.5 times higher generation rate as compared to silicon dioxide samples. As a result, for the same dose, the number of electron-hole pairs produced in silicon nitride is twice as much as in silicon dioxide. The trapping mechanism involved in silicon nitride samples is discussed in [22, 23]. Even though the generation rate is higher for silicon nitride samples, the dose sensitivity also depends on the number of precursor defect densities where the holes can be trapped.

5.2.1 Experiment results

Figs. 27 and 28 show the experimental data obtained from ^{60}Co irradiation experiment. The C-V curves suggests that the silicon nitride samples show saturated levels at a dose of 100 krad while the silicon dioxide samples show linear increase up to 300 krad. This suggests that the dynamic range of silicon nitride samples is less than the silicon dioxide counterparts.

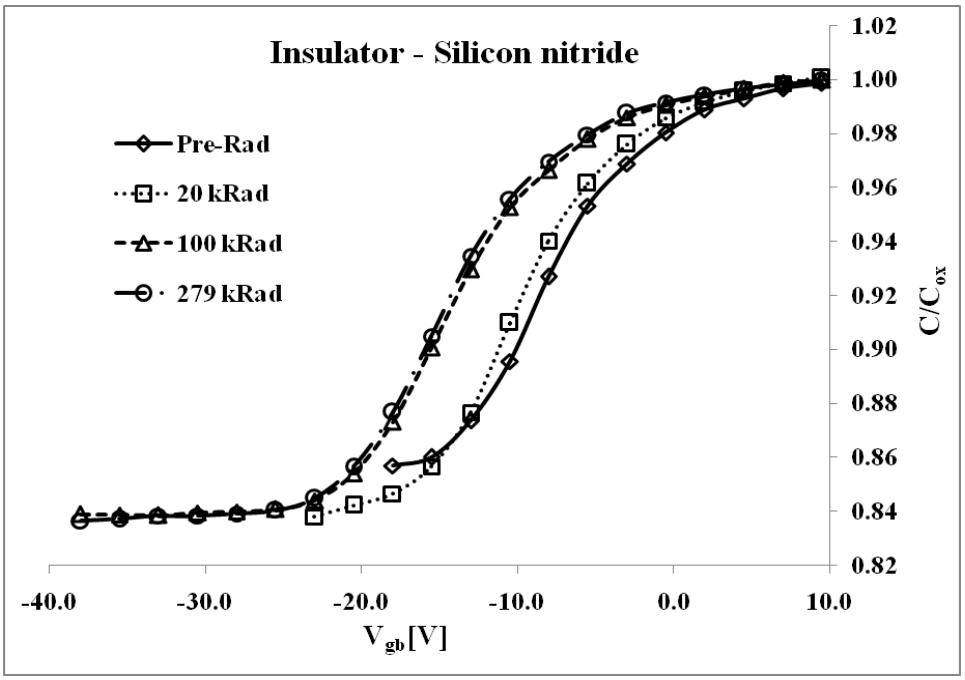

Fig. 27. Pre-irradiation and post-irradiation C-V curves of RADCAP with silicon nitride as insulator

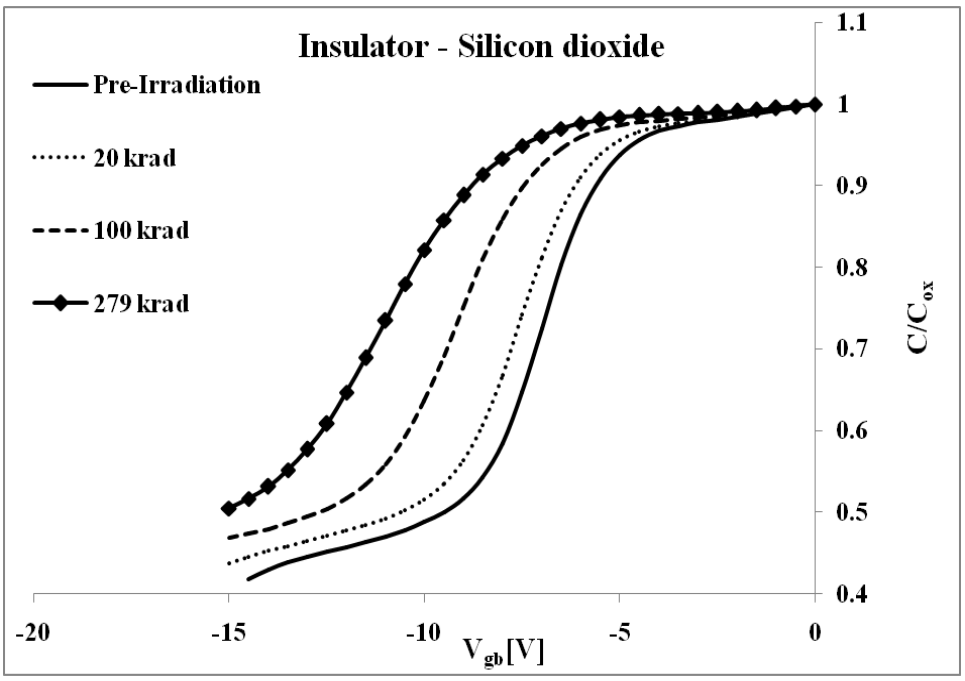

Fig. 28. Pre-irradiation and post-irradiation C-V curves of RADCAP with silicon dioxide as insulator

In order to compare their efficiency as dose sensors, the change in oxide-trapped charge was extracted as a function of dose and normalized with respect to oxide thickness. The data of silicon dioxide samples were corrected to take fractional hole yield into account. It can be seen from Fig. 29 that silicon dioxide samples show more change in oxide-trapped charge ΔN_{OT} for the same dose levels than silicon nitride samples. Also the silicon nitride samples show no shift in the C-V curve after the 100 krad indicating that its dynamic range is limited by the number of trapping sites.

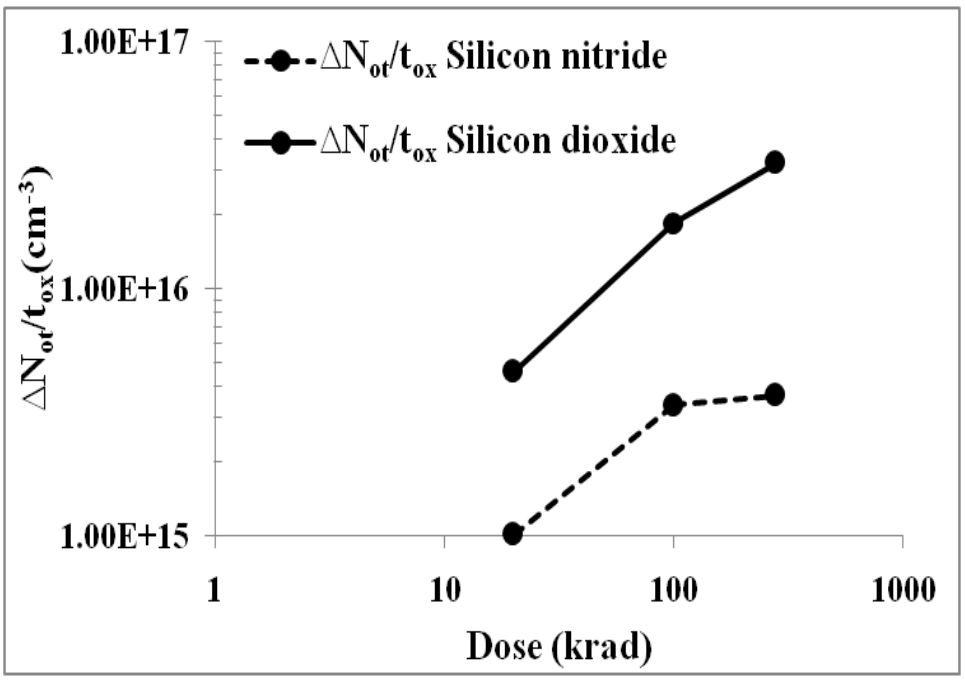

Fig. 29. Comparison of normalized oxide-trapped charge density of silicon nitride and silicon dioxide RADCAP samples as a function of dose

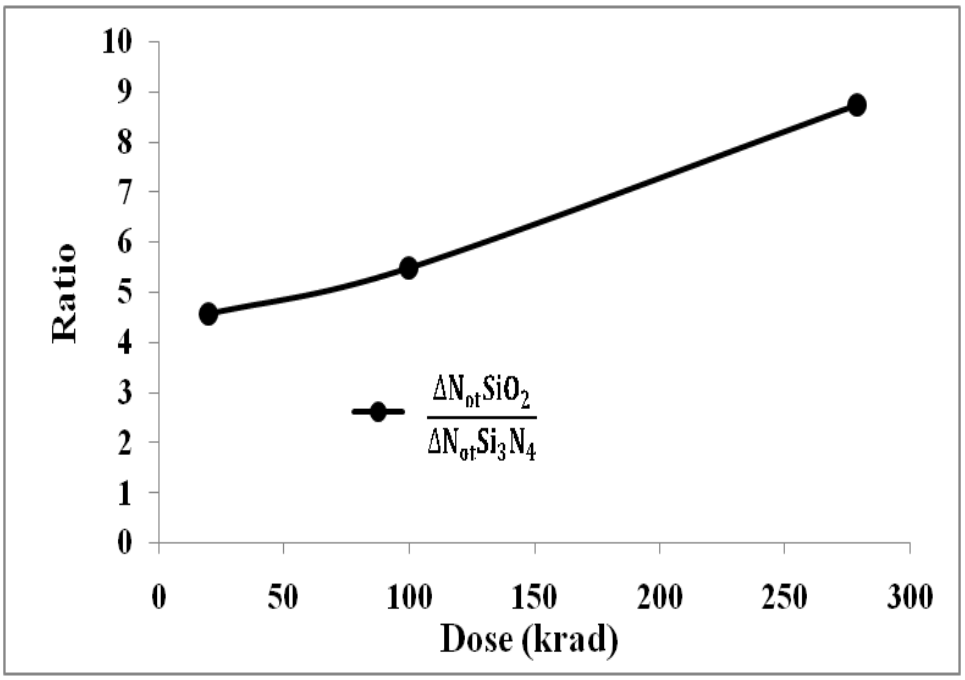

Fig. 30. Ratio of normalized oxide-trapped charge density of silicon dioxide and silicon nitride RADCAP samples as a function of dose

Shown in Fig. 30 is the ratio of oxide-trapped charge density of silicon dioxide and silicon nitride samples. It can be seen that the ratio is monotonically increasing indicating that the oxide samples show more trapping efficiency than the silicon nitride samples even at higer dose levels. It is thus recommended to use silicon dioxide when the dose sensor is to be used for high dose levels. Although silicon nitride requires lower energy for electopn-hole pair generation reduced number of trapping sites impacts its dose sensitivity. It can be seen from the C-V curves that both silicon dioxide and silicon nitride samples show very little interface trap charge. The stretch out of the curves from midgap to inversion is almost the same at all dose levels. The initial precursor hole trap density in the silicon nitride sample is estimated using the REM module of Silvaco device simulator to be $4 \times 10^{17} cm^{-3}$.

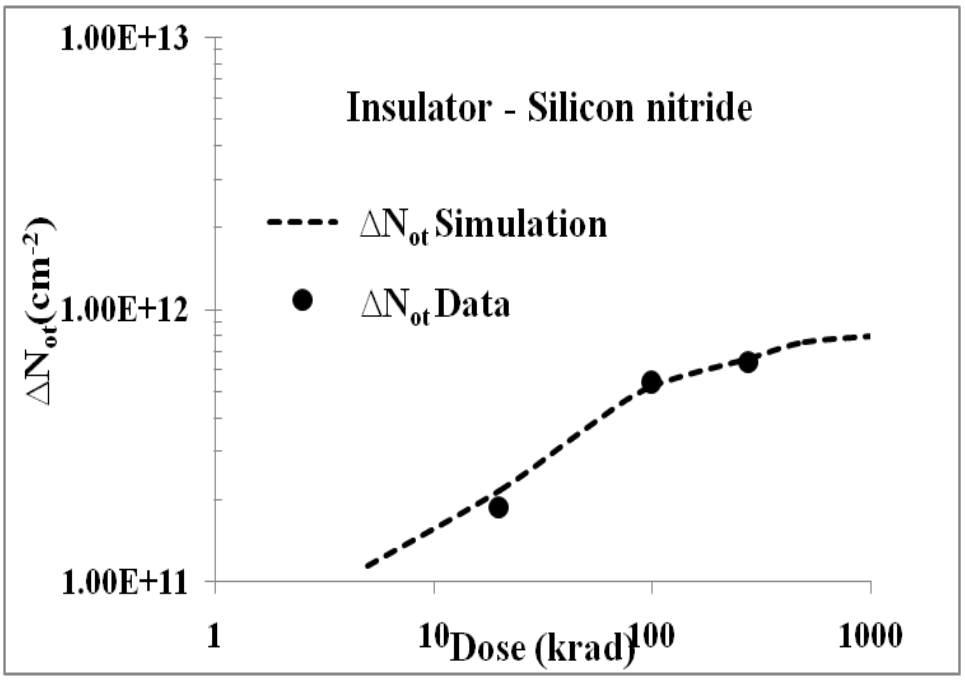

Fig. 31. Comparison of oxide-trapped charge per unit area for silicon nitride RADCAP obtained from simulation and experimental data

Fig. 31 compares the oxide-trapped charge obtained using simulation and experiments for the silicon nitride samples. The simulation results match closely with the experimental data validating the initial precursor hole trap density estimated using simulations is close to experimental value.

5.3 Impact of oxide thickness

Thickness of oxide is a critical parameter that affects the total oxide-trapped charge density in the sample [3-7]. The radiation induced midgap voltage shift, ΔV_{mg} is directly proportional to t_{ox}^2 [11] and this follows from the basic equation, Q = CV. The charge, Q is proportional to t_{ox} while C is inversely proportional to t_{ox}. In order to improve the dynamic range of the dose sensor, the change in capacitance at fixed bias should continue for widest range of dose levels. This presents a tradeoff between dose sensitivity and dynamic range. The thickness of oxide should be small to improve the dynamic range so that for the same increase in dose level, the change in midgap voltage is less which reflects in small ΔC change. But the thinner oxide is more radiation hardened as compared to the thicker oxide.

5.3.1 Experiment results

The change in oxide-trapped charge and interface trap density were extracted from experimental data and normalized with respect to fractional hole yield $f_y(E_{ox})$. Figs. 32 and 33 compare the normalized oxide-trapped charge and interface trap density for RADCAP samples with 100 nm and 200 nm oxide thickness.

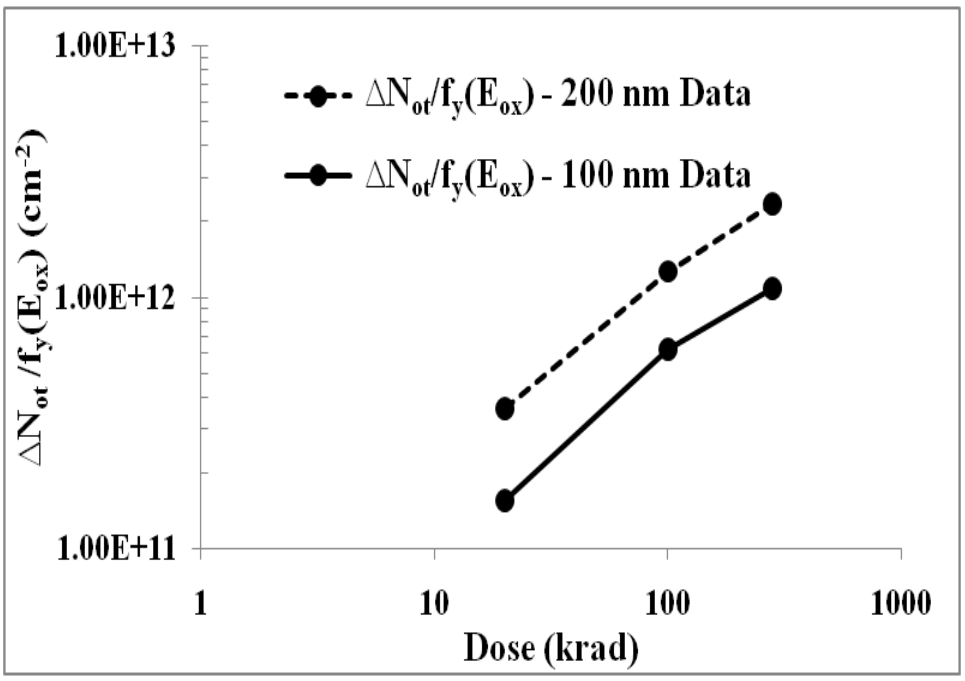

Fig. 32. Comparison of normalized oxide-trapped charge per unit area for RADCAPs with 100 nm, 200 nm oxide thickness as a function of dose

From Figs. 32 and 33 it can be seen that the 200 nm samples show both higher interface traps as well as more oxide-trapped charge. It can be clearly seen that the 200 nm oxide samples are more radiation sensitive, trapping more oxide charge as compared to their 100 nm counterparts for the same dose levels. Also the thicker oxide has more interface traps that affect the shape of the C-V curve and thereby impacting the dose sensor's performance. Previous studies indicate that the radiation induced interface trap density is reduced in thinner oxides [24-30]. So in the thinner oxides, the amount of interface traps produced even at very large doses is less.

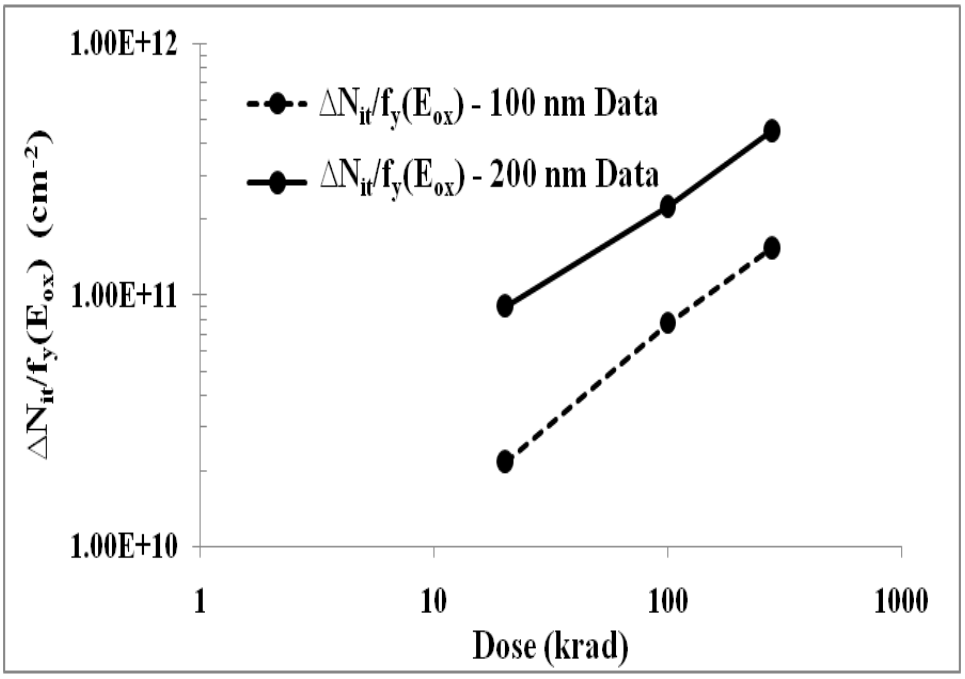

Fig. 33. Comparison of normalized interface state charge per unit area for RADCAPs with 100 nm, 200 nm oxide thickness as a function of dose

5.4 Post-irradiation behavior

An effective dose sensor should hold the charge in its insulator layer even after irradiation stops and should present very little charge loss over time. In order to characterize the sensors manufactured using different processing techniques, the samples were annealed at room temperature with no bias after exposing them to ionizing radiations. Fig. 34 shows the post irradiation annealing behavior observed in different samples. It can be seen that all the samples show loss of oxide-trapped charge irrespective of their processing scheme. The capacitors manufactured using dry oxidation and wet oxidation show annealing of interface traps produced during irradiation and loss of oxide-trapped charge.

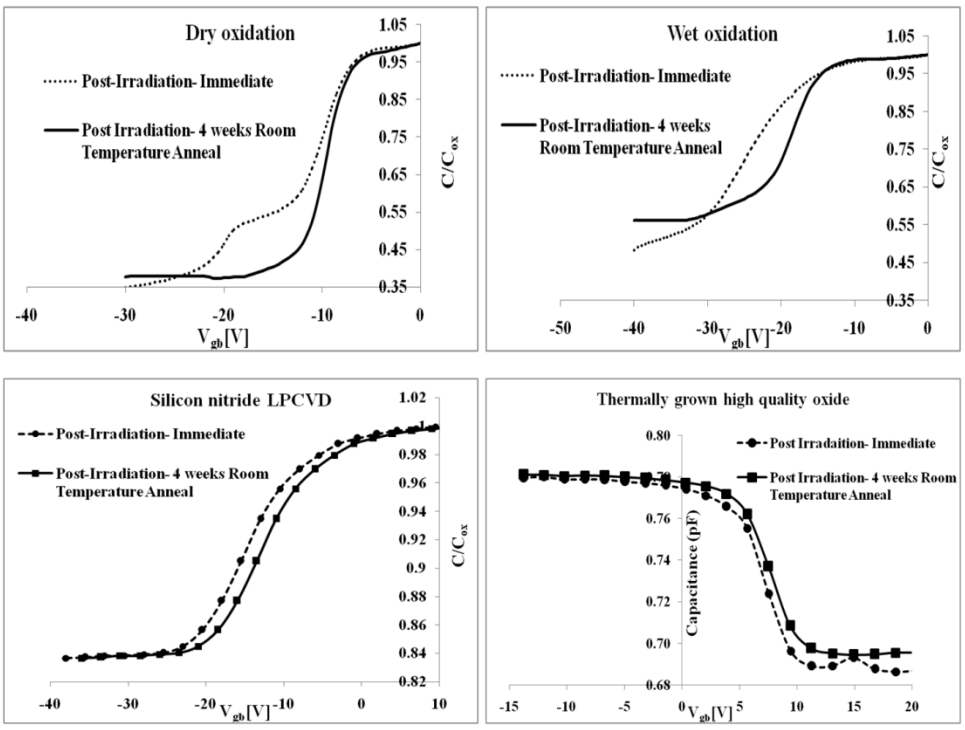

Fig. 34. Comparison of annealing behavior observed in RADCAPs manufactured using different processing techniques

The reason for annealing is that the fields produced due to oxide-trapped charge cause electrons to be injected from the substrate that compensates the trapped holes thereby causing the flat-band voltage to recover. Table 4 summarizes the loss of oxide-trapped charge and midgap voltage shifts resulting from room temperature annealing. In order to improve the dosimeter, the loss of oxide-trapped charge over time has to be reduced.

INSULATOR TYPE	PROCESSING TECHNIQUE	MIDGAP VOLTAGE SHIFT, $\|\Delta V_{mg}\|$, V	OXIDE-TRAPPED CHARGE LOST DUE TO ANNEALING, ΔN_{OT}, cm^{-2}
SiO_2	Wet Oxidation	4.5	4.85×10^{11}
SiO_2	Dry Oxidation	2.5	5.39×10^{11}
Si_3N_4	Chemical Vapor Desposition	2	5.19×10^{10}
SiO_2	Industry grown thermal oxide	1	1.08×10^{10}

Table 4. Loss of oxide-trapped charge and midgap voltage shifts resulting from room temperature annealing

5.5 Discussion on initial precursor hole trap density

The initial precursor hole trap density in the oxide can provide a fair comparison of sensitivity of dose sensor to radiation. It helps to understand the radiation dose sensitivity of different materials and various processing schemes. The initial precursor hole trap density determines the rate of buildup of trapped charge in insulator and dose level at which the buildup saturates. It predicts the dynamic range of dose levels for which the dose sensor would provide a change in capacitance thereby working as a radiation dose sensor. The initial precursor hole trap density estimated using simulations are summarized in Table 5

INSULATOR TYPE	PROCESSING TECHNIQUE	INITIAL HOLE TRAP DENSITY, cm^{-3}
SiO_2	Wet Oxidation	10^{18}
SiO_2	Dry Oxidation	10^{18}
Si_3N_4	Chemical Vapor Desposition	4×10^{17}
SiO_2	Industry grown thermal oxide	1.5×10^{16}

Table 5. Initial precursor hole trap density estimated from simulation for various processing schemes

The simulation results suggest that the initial precursor hole trap density is same for the natively grown silicon dioxide samples, irrespective of their processing method. Thermal oxides grown in the industry have initial precursor hole trap density that is two orders of magnitude lower when compared to the samples grown at ASU. The silicon nitride samples prepared using CVD technique has about 2.5 times lower initial precursor hole trap density as compared to the silicon dioxide samples grown at ASU. The estimate of initial precursor hole trap density is important as it predicts the dynamic range for which the MOS capacitor continues to develop oxide-trapped charge thereby providing a capacitance change. The precursor hole trap density influences the sensitivity of the insulator to radiation in addition to other parameters like temperature, electric field, oxide thickness. Since the RADCAP is used in an unbiased condition its sensitivity is critically influenced and controlled by the initial precursor hole trap density in the insulator.

The RADCAP can be used as a wireless dose sensor if the parameters described above can be controlled efficiently. The advantage of this system is that it is passive, low cost, small and easy to manufacture. It incorporates all the advantages of RADFET in addition to providing a wireless method to sense radiation. With the need for cheap wireless radiation sensing getting impetus, this technique can provide robust wireless radiation dose sensors.

Chapter 6

CONCLUSION

The effect of oxide processing scheme, choice of insulator material and oxide thickness have been studied. Wet oxidation and dry oxidation introduce the same number of initial precursor hole trap density which characterizes the oxide-trapped charge build-up. Due to the presence of water species, wet oxidation introduces slightly higher levels of interface traps at the same dose levels as compared to dry oxidation. Radiation response of industry grown thermal oxides show reduced amount of initial precursor hole trap density as compared to natively grown counterparts. The impact of silicon nitride as insulator material in the place of oxide showed saturated levels of oxide-trapped charge at a radiation dose of 100 krad which severely impact the dynamic range of the dose sensor. In order to use the sensor at high dose levels, the rate of build-up of oxide-trapped charge should be small thereby continuing to show a change in capacitance detectable at higher dose ranges. A tradeoff exists between dynamic range and thickness of oxide in building a radiation dose sensor. A thicker oxide is much more radiation sensitive than thinner oxide but saturates much earlier than similarly processed thinner oxide thereby having a reduced dynamic range. It is necessary to understand this tradeoff in order to build RADCAP dosimeter for various applications.

REFERENCES

[1] R.C.Hughes , "Theory of response of radiation sensing field-effect transistors in zero bias operation",*J.Appl Phys,* Vol 60, 1216-1217, 1986

[2] A.G. Holmes-Siedle, "The space charge dosimeter: general principle of a new method of radiation dosimetry",*Nucl Instrum Meth,*pp 169-179, 1974

[3] A.G. Holmes-Siedle, Leonard Adams,"RADFET: A review of the use of Metal-Oxide-Silicon devices as integrating dosimeters",*Rad. Phys and chem,* Vol 28, no.2, pp 235-244, 1986

[4] G.Ristic,S. Golubovic and M.Pejovic,"pMOS transisitors for dosimetric applications",*Electron. Lett, Vol 29, pp 1644-1646, 1993*

[5] G.Sarrabayrouse and S.Siskos,"Radiation dose Measurements using MOSFETs", *IEEE Instr and Mes Magazine, pp 26-34, 1998*

[6] N.Kumurdjian and G.Sarrabayhouse,"Unbiased Metal Oxide Semiconductor ionising radiation dosimeter", *Rad. Protection Dosimetry,Vol 61, pp 19-24, 1995*

[7] A.G. Holmes-Siedle, Paul Menary, Phil Sharpe, John.A.Mills,"RADFET devices are they coming of age?", *Scope*, pp 21-27, 2010

[8] A. Holmes-Siedle, L. Adams and G. Ensell," MOS dosimeters - improvement of responsivity",*Rad and its Effects on Dev and Sys, pp 65-69, 1991*

[9] M.Soubra, J. Cygler and G.Mackay," Evaluation of a dual bias dual metal oxide-silicon semiconductor field effect transistor detector as radiation dosimeter", *Med Phys,* Vol 21, pp 567-572, 1994

[10] H.P.Hjalmarson, R.L.Pease, S.C.Witczak, M.R.Shaneyfelt, J.R.Schwank, A.H.Edwards, C.E.Hembree, and T.R. Mattsson, “Mechanisms of radiation

dose-rate sensitivity of bipolar transistors," *IEEE Trans Nucl. Sci,* vol. 50, p.1901, 2003

[11] T.R.Oldham,"Total Ionizing Dose Effects in MOS Oxides and Devices",*IEEE Trans on Nucl Sci,* Vol 50, pp 483-499, 2003

[12] Craig Casey Jr,"Devices for Integrated Circuits",*John Wiley & Sons Inc,*1999

[13] P.S.Winokur, J.R. Schwank, P.J. Mcwhorter, P.V. Dressendorfer, and D.C. Turpin,"Correlating the radiation response of MOS capacitors and transistors",*IEEE Trans on Nucl Sci,* Vol NS-31, pp 1453-1460, Dec 1984

[14] F.B.Mclean,"A Framework For Understanding Radiation-Induced Interface States in Sio_2 MOS Structures",*IEEE Trans.Nucl.Sci.,*vol. NS-27, no.6,pp.1651-1657, Dec1980

[15] C.T. Sah, *IEEE Trans. Nucl. Sci.,* NS-23, pp.1563-68, Dec. 1976

[16] I.G. Batyrev, D.M.Fleetwood, R.D.Schrimpf, S.T.Pantelides,"The role of water in the radiation response of wet and dry oxides", *Rad and its effects on Components and Sys.*, pp 1-6, Sept 2007

[17] S. N. Rashkeev, D. M. Fleetwood, R. D. Schrimpf, and S. T. Pantelides, "Effects of hydrogen motion on interface trap formation and annealing," *IEEE Trans Nucl. Sci.,* vol. 51, pp. 3158-3165, 2004

[18] N. S. Saks and D. B. Brown, "Interface trap formation via the two-stage H process," *IEEE Trans. Nucl. Sci.*, vol. 36, no. 6, pp. 1848–1857, Dec. 1989

[19] P. S.Winokur and H. E. Boesch, Jr., "Interface-state generation in radiation-hard oxides," *IEEE Trans. Nucl. Sci.*, vol. NS-27, p. 1647, 1980S. N. Rashkeev, D. M. Fleetwood, R. D. Schrimpf, and S. T. Pantelides, "Effects of hydrogen motion on interface trap formation and annealing," *IEEE Trans Nucl. Sci.*, vol. 51, pp. 3158-3165, 2004

[20] H.Edwin Boesch Jr , F. Barry Mclean, “Hole Transport and Trapping in Field Oxides,"*IEEE Trans Nucl Sci*,vol NS-32, no.6, Dec 1985

[21] G. C. Messenger, M. S. Ash,"The Effects of Radiation on Electronic Systems", *2nd edition, Van Nostrand Reinhold*, NY, 1992.

[22] Bob H Yun,"Electron and hole transport in CVD Si3N4 films", Appl Phys Letters, Vol 27, pp 256-258, 1975

[23] Z.A.Weinberg,"Hole Conduction in Si3N4 films on Si", Appl Phys Letters, Vol 29, pp 617-619, 1976

[23] Z.A.Weinberg,"Hole Conduction in Si3N4 films on Si", Appl Phys Letters, Vol 29, pp 617-619, 1976

[24] K.Naruke, M.Yoshida, K.Maeguchi and H.Tango,”Radiation-Induced Interface States of Poly-Si Gate MOS Capacitors using Low Temperture Gate Oxidation”,IEEE Trans on Nucl. Sci,NS-30, pp 4054-58, 1983

[25] J.M.Benedetto,H.E.Boesch,F.B.Mclean,"Hole Removal in thin-gate MOSFET by Tunneling", *IEEE Trans on Nucl. Sci*,NS-32, pp 3916-20, 1985

[26] T.P.Ma,"Oxide thickness dependence of electron- induced surface states in MOS structures",Appl Phys Letter,Vol 27, pp 615

[27] C.R.Viswanathan, J.Maserjian," Model for Thickness Dependence of Radiation Charging in MOS Structures", *IEEE Trans on Nucl. Sci*,NS-23, pp 1540-45, 1976

[28] N.S.Saks, M.G. Ancona and J.A. Modolo," Generation of Interface States by Ionizing Radiation in Very Thin MOS Oxides", *IEEE Trans on Nucl. Sci*,NS-33, pp 1185-90, 1986

[29] S.Share, A.Epstein, V.Kulmar, W.E. Dahlkeand W.Haller,"Effects of Ionizing Radiation on the thin oxide (20-1500Å)",J. Appl Phys,Vol 45, pp 4894

[30] T.P.Ma and R.C. Barker,"Effect of gamma-ray irradiation on the surface states of MOS tunnel junctions",J. Appl Phys,Vol 45, pp 317